

PHOTOGRAPH THIS SHEET

AD-A193 917

DTIC ACCESSION NUMBER

LEVEL

LEVEL

INVENTORY

INVENTORY

MRC/WDC-R-025

DOCUMENT IDENTIFICATION

MAY 1982

This document has been approved for public release and since its distribution is unlimited.

DISTRIBUTION STATEMENT

ACCESSION FOR

NTIS GRA&I

DTIC TAB

UNANNOUNCED

JUSTIFICATION

BY

DISTRIBUTION /

AVAILABILITY CODES

DIST

AVAIL AND/OR SPECIAL

A-1

DISTRIBUTION STAMP



DTIC ELECTED
S JUN 13 1988 D
E

DATE ACCESSIONED

DATE RETURNED

DATE RETURNED

DATE RECEIVED IN DTIC

DATE RECEIVED IN DTIC

REGISTERED OR CERTIFIED NO.

REGISTERED OR CERTIFIED NO.

PHOTOGRAPH THIS SHEET AND RETURN TO DTIC-FDAC

Copy No. 5

MRC/WDC-R-025

High Power Microwave Interaction With Air

W. M. Bollen
C. L. Yee
M. J. Nagurney

May 1982

Prepared for: Naval Research Laboratory
4555 Overlook Avenue, S. E.
Washington, D. C. 20380

Contract No. N00014-81-C-2105

Prepared by: MISSION RESEARCH CORPORATION
5503 Cherokee Avenue, Suite 201
Alexandria, Virginia 22312
(703) 750-3556

APPROVED FOR PUBLIC RELEASE
DISTRIBUTION UNLIMITED

REPORT DOCUMENTATION PAGE		READ INSTRUCTIONS BEFORE COMPLETING FORM	
1. REPORT NUMBER	2. GOVT ACCESSION NO.	3. RECIPIENT'S CATALOG NUMBER	
4. TITLE (and Subtitle) Investigation of High-Power Microwave Breakdown in Air		5. TYPE OF REPORT & PERIOD COVERED Final Report 21 Jan 1981 - 20 Jan 1982	
7. AUTHOR(s) W. M. Bollen M. J. Nagurney C. L. Yee		6. PERFORMING ORG. REPORT NUMBER MRC/WDC-R-025	
9. PERFORMING ORGANIZATION NAME AND ADDRESS Mission Research Corporation 5503 Cherokee Avenue, Suite 201 Alexandria, Virginia 22312		8. CONTRACT OR GRANT NUMBER(s) N00014-81-C-2105	
11. CONTROLLING OFFICE NAME AND ADDRESS Naval Research Laboratory 4555 Overlook Avenue, S. E. Washington, D. C. 20370		10. PROGRAM ELEMENT, PROJECT, TASK AREA & WORK UNIT NUMBERS	
14. MONITORING AGENCY NAME & ADDRESS (if different from Controlling Office)		12. REPORT DATE May 1982	
		13. NUMBER OF PAGES	
		15. SECURITY CLASS (of this report) UNCLASSIFIED	
		15a. DECLASSIFICATION/DOWNGRADING SCHEDULE N/A	
16. DISTRIBUTION STATEMENT (of this Report) Naval Research Laboratory, Code 4740 (1 copy) DCASMA, Oxnard (1 copy) Naval Research Laboratory, Code 2627 (6 copies) DDC, Code S47031 (12 copies) NAVAIR, Code 350F (1 copy)			
17. DISTRIBUTION STATEMENT (of the abstract entered in Block 20, if different from Report) APPROVED FOR PUBLIC RELEASE DISTRIBUTION UNLIMITED			
18. SUPPLEMENTARY NOTES			
19. KEY WORDS (Continue on reverse side if necessary and identify by block number) Microwave Air Breakdown Interaction Reflection N ₂ Breakdown Coupling Absorption High Power			
20. ABSTRACT (Continue on reverse side if necessary and identify by block number) The computer simulation code MINI has been developed to study microwave interaction with nitrogen. MINI has self-consistent wave optics, nitrogen chemistry and hydrodynamic effects included. A number of simulations have been performed and compared to experiment showing reasonable agreement.			

CONTENTS

<u>Section -</u>	<u>Page</u>
I INTRODUCTION	1
II CODE DEVELOPMENT	2
III QUALITATIVE FEATURES OF GAS BREAKDOWN	4
IV COMPARISON OF EXPERIMENT TO MINI	6
REFERENCES	8
APPENDIX A	
APPENDIX B	
APPENDIX C	

ILLUSTRATIONS

Figure

Page

1

Comparison of Experiment and Simulation for Electron
Density

7

I. INTRODUCTION

For the past year Mission Research Corporation has been pursuing a computational and theoretical investigation of high power microwave interactions with air for the Naval Research Laboratory. The technical objectives were to design, construct, operate and benchmark against experimental data a one-dimensional, self-consistent computer simulation of microwave breakdown of nitrogen. A self-consistent nitrogen chemistry-wave optics hydrodynamic Microwave Gas Breakdown simulation code MINI has been developed. We have used MINI to simulate the MRC experiments being performed for NRL (ref. 1) and also to study the microwave-plasma coupling from atmospheric to low (25 Torr) pressure.

Preliminary simulations have been performed with a simplified version of MINI which excludes hydrodynamic motion of the electrons and the neutral gas. The qualitative features of these "No-Hydro" simulations appear to be consistent with experimental results. These preliminary simulations are extremely useful, since they allow both hydrodynamic effects and effects due to plasma reflectivity to be easily isolated. The No-Hydro simulations were used primarily to study the reflection and absorption of the microwaves with the breakdown gas. This is an approximation even for short pulses since the neutral gas requires only a small drift speed to conduct/convect large amounts of energy out of a region. In principle MINI could be run for very long times to follow the neutral gas motion; however, times much larger than 1 μ sec become costly.

In the course of investigation, the electron density profile was seen to be reasonably modeled using either a symmetric or slab model profile. Using a slab model for the electron density profile allowed a simple simulation to be performed using a separately developed long-term chemistry code. The issue addressed in these long-term chemistry simulations (LTCS) was the reflectivity of the breakdown plasma due to thermal ionization of the neutral gas. In a thermodynamic equilibrium, with a gas temperature of one electron volt, the breakdown plasma would

reflect essentially all of the incident microwave energy. These simulations were typically run for tens of microseconds and provided valuable quantitative insight into gas heating by microwave radiation. In what follows, a brief synopsis of the code development and the theory to date on microwave gas breakdown will be discussed.

II. CODE DEVELOPMENT

The primary objective in fiscal year 1981 was the development of a self-consistent nitrogen chemistry - wave optics - hydrodynamic simulation to investigate microwave decoupling due to gas motion. However, research was initiated using a wave optics chemistry code to address the issue of plasma reflectance from a high density plasma. The results showed that the energy deposition of the microwave could not be sufficiently localized to heat the gas. The details of the wave optics chemistry code are given in Appendix A. The code follows the electric field by solving the wave equation for a plane wave of normal incidence. The electromagnetic boundary conditions were of the Lindman (Ref. 2) type. The electric field provides the energy source for the 11 species nitrogen chemistry code, CHEMN2, developed for this project. CHEMN2 calculates the time development of ground state molecular nitrogen, atomic nitrogen, their first charge state, the excited states, $N_2^+(B)$, N_4^+ , $N(^2D)$, $N_2(A)$, $N_2(B)$, $N_2(C)$; and the electrons. The heavy particle temperature, T_g , vibrational temperature, T_v , and the electron temperature, T_e , are also calculated. The set of stiff differential equations are solved using a modified version of CHEMEQ (Ref. 3). The wave optics code has been thoroughly tested and is used extensively in the simulation of the short pulse experiments.

The development of the hydrodynamic, nitrogen chemistry and wave optics simulation MINI (Microwave Nitrogen Interaction Code) was completed in early 1982. As an extension of the wave optics chemistry simulation MINI follows the hydrodynamics of the previous mentioned species. Transport processes for the gas include viscous heating and thermal conduction. The transport coefficients were taken from Bird (Ref. 4 and

5). A Eulerian differential equation of the hydrodynamic equation in conservative form is solved using the algorithm of Rubin and Burstein (Ref. 6). The scheme is simple, second order in accuracy, and is relatively stable while centering the dissipation terms. Although no use is made of any artificial viscosity, the code can be switched to use the Flux-Corrected-Transport (FCT) algorithm of Boris (Ref. 7). The hydrodynamic and chemistry portions are calculated separately in a cycle assuming sufficiently weak flows. The hydrodynamics is determined from the updated values of the chemistry. Hence, the hydrodynamics is considered as a small correction to the chemistry.

MINI follows both the electrons and gas hydrodynamics in a two fluid model assuming separate fluids for the electrons and the heavy particles. The continuity equation for each species is solved. A single mass-average velocity for the heavy particles is calculated. The diffusion of the neutral species is neglected except for the dominant molecular nitrogen species. The contribution from the electric field is included in describing the diffusion of the charged species. The DC electric field is assumed to be ambipolar with the sum of the positively charged particle flux equal to the electron particle flux. In the strongly collisional region, the electrons do not sample regions of different electric field or pressure. We assume the electrons are in steady state as are the positively charged species. The ambipolar field assumption allows for the solution of the ambipolar field and the electron drift speed. Sources which cool the electrons and, therefore, heat the positively charged particles and, hence, the gas include the following terms: joule heating by AC and DC electric fields, elastic and inelastic heating, and work due to momentum transfer. Since the translational and rotational degrees of freedom of the heavy particles are closely coupled and are in near equilibrium, only an energy equation describing the vibrational energy and translational energy of the gas is included. Hence, the three energy equations solved are for the electrons, heavy particles, and the total vibrational energy.

The AC electric field can be solved in the regular planar geometry or in spherical geometry. However, the hydrodynamics and chemistry are always solved in a one dimensional planar geometry. The solution of the spherical wave equation is used only in modeling spherical or focused systems similar to the MRC/NRL experiments. The solution to the hydrodynamic equations in planar geometry and the solution to the wave equation in spherical geometry are not consistent. One can easily imagine systems in which the lateral scale lengths of the system are long compared to the longitudinal (parallel to the propagation vector) scale lengths. In such systems, diffusion would actually occur most rapidly in the longitudinal direction or radial direction if calculating the electric field in spherical geometry.

MINI can also be run using a dilated electron mass. This allows for longer time steps in the chemistry and hydrodynamics. Dilating the electron mass can be justified physically when the electron drift speed is slow, i.e., the kinetic energy is small compared to the electron temperature. As mentioned previously, the hydrodynamics is taken as a correction to the chemistry. Hence, in the chemistry portion of the calculation, the real electron mass is explicitly used.

III. QUALITATIVE FEATURES OF GAS BREAKDOWN

Based on simulations using MINI, we have documented some qualitative features of microwave breakdown of gases. The first of these is microwave energy coupling to the breakdown plasma. One general characteristic of microwave coupling to a breakdown plasma is the inability to localize the energy deposition. The problem of interest requires the gas to be significantly heated before the microwave energy decouples. Further gas heating, as in a slow combustion wave (in which the gas diffusion time is comparable to the gas heating time), is to be distinguished from a fast detonation wave (in which the gas diffusion time is long compared to the gas heating time.) The latter may have substantial military applications. The basic question addressed was under

what circumstances can a large amount of microwave energy be deposited rapidly into the gas. Under high irradiance, the electron density rises sufficiently rapidly to partially reflect the incident radiation. The total electric field then proceeds to break down the gas at a position away from the instantaneous peak electron density in the direction of the source (anti-parallel to the wave vector). This secondary ionization rises rapidly to absorb the microwaves and shields (decouples) the primary ionization front from the microwave radiation. This then limits the deposition time of the radiation into the gas. Secondary ionization fronts due to this process were observed in preformed plasmas or plasmas formed in a highly spherical (focused) system.

The primary gas heating mechanism at relatively high pressures (greater than 25 Torr) in nitrogen is quenching of the electronic states by molecular and atomic nitrogen. Hence, rapid gas heating requires high electron density and temperature, sufficiently high to excite the electronic states through electron impact. Full hydrodynamic simulations of short pulse nitrogen breakdown experiments with no target have shown that the gas is not sufficiently heated to excite these states. Simulations show electron temperatures on the order of 1-2 eV and an electron density on the order of $1 \times 10^{13} \text{ cm}^{-3}$ for the 35 GHz experimental parameters. The electric field is rapidly attenuated in a distance of approximately one wavelength. The results are expanded in more detail in Appendix B. These simulation results are qualitatively consistent with the experiment.

Simulation of microwaves incident on a reflecting surface show breakdown occurring at the peak nodes of the electric field (the characteristic standing wave pattern), as would be expected. As the electron density rises, these "pancakes" of electron density begin to attenuate the radiation such that the pancake closest to the reflecting surface (one-quarter wavelength away) is shielded from the radiation. As the absorption continues, the remaining pancakes would then sequentially decouple the next pancake closest to the surface, and the process repeats itself. Again, in these low pressure simulations, the gas is not significantly heated.

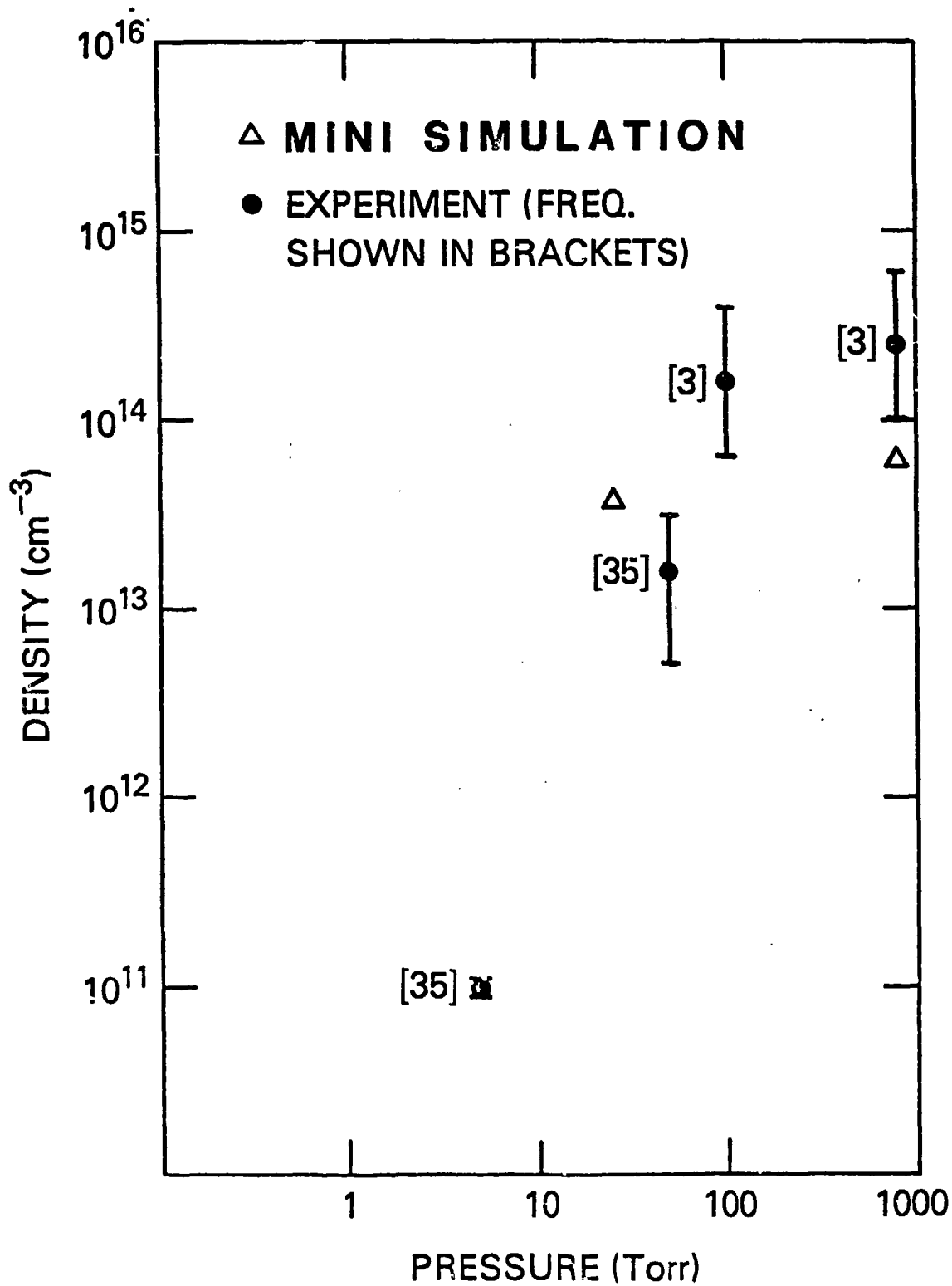
IV. COMPARISON OF EXPERIMENT TO MINI

Comparison of MINI to the NRL/MRC experiments has been undertaken to verify that MINI includes the proper physics to simulate microwave breakdown of nitrogen. Comparison of the simulation predictions and experimental measurements of electron density are shown in Figure 1. This data is based on both 3 GHz and 35 GHz experiments. Agreement is good, degrading towards the high pressure region. One explanation for this discrepancy is that MINI assumes a Maxwellian distribution for the electrons. This assumption, particularly for the tail electrons which do the ionization, may not be valid for $v/\omega > 1$ (high pressure).

Experimental observations of the spectra have been unable to detect the N_2^+ 3914Å band. Only the second positive neutral nitrogen bands have been observed. This is consistent with MINI's prediction of $I_{3914}/I_{3371} = 10^{-4}$ for the experimental parameters. This effectively sets an upper bound on the electron temperature in the experiment, $T_e \leq 2$ eV.

Finally, ionization fronts such as those predicted by MINI were observed. This is discussed in detail in Appendix C where a copy of our upcoming article is reproduced.

COMPARISON OF EXPERIMENT AND SIMULATION FOR ELECTRON DENSITY



REFERENCES

1. W. M. Bollen, R. K. Parker, and W. M. Black, "Experiments on the Interaction of Highpower Microwaves with Air," MRC/WDC-R-015, (July 1981).
2. E. L. Lindman, "Free-Space Boundary Conditions for the Time Dependent Wave Equation," J. Computational Phys. 19, 66 (1975).
3. T. R. Young, Jr., "CHEMEQ - A Subroutine for Solving Stiff Ordinary Differential Equations," NRL Memorandum Report No. 4091 (1980).
4. R. B. Bird, "Transport Phenomena," Wiley Press, New York (1960).
5. J. M. Picone and E. S. Oran, "Approximate Equations for Transport Coefficients of Multicomponent Mixtures of Neutral Gas," NRL Memorandum Report 4384 (1980).
6. E. L. Rubin and S. Z. Burstein, "Difference Methods for the Inviscid and Viscous Equations of a Compressible Gas," J. Computational Phys. 2, 178, (1967).
7. D. L. Book, J. P. Boris, and K. Hain, "Flux-Corrected Transport II: Generalization of the Method," J. Computational Phys. 18, 248, (1975).

APPENDIX A

C

C

C

C

Microwave Energy Deposition, Breakdown and Heating of Nitrogen

C. L. Yee
Mission Research Corporation

A. W. Ali
Naval Research Laboratory

ABSTRACT

A comprehensive code is developed for the microwave energy deposition in N_2 to describe the breakdown and heating of nitrogen. The microwave absorption and reflection from a nitrogen plasma is based on wave optics. The ionization and the deionization of N_2 , however, is described in detail by an N_2 chemistry code (CHEM- N_2) which provides plasma diagnostics capabilities by calculating emission intensities of the second positive and the first negative band systems of N_2 and N_2^+ .

The code is applied to breakdown calculations in N_2 and the results are in reasonable accord with experimental data. The wave optics code for energy deposition is also coupled to an air chemistry code (CHMAIR) to describe the breakdown off a reflecting surface.

An insight is provided into the plasma absorption by using a simple slab density profile for the electrons. This models roughly the profile expected in air breakdown off a reflecting surface. Simulation results show a steep localized electron density profile at the interference maximum. These simple calculations show the plasma reflectivity to be small ($< 25\%$) for 1 cm light at high electron densities, $N_e \gg 10^{15} \text{ cm}^{-3}$ $N_c = 10^{13} \text{ cm}^{-3}$. Simulation results also show the possibility of attaining high electron density. However, in breakdown off a reflecting surface, the microwave is decoupled from the plasma when the absorption length is less than one-half the wavelength of the light. Important questions to be addressed in the future include the possibility of plasma maintenance, gas heating, shock formation, plasma decoupling and effects of strong non-linear forces.

CONTENTS

1. INTRODUCTION	1
2. THE E AND M CODE	2
3. N ₂ BREAKDOWN AND OPTICAL DIAGNOSTICS	6
4. APPLICATIONS TO BREAKDOWN STUDIES	19
REFERENCES	29

MICROWAVE ENERGY DEPOSITION, BREAKDOWN AND HEATING OF NITROGEN AND AIR

I. INTRODUCTION

The interactions of the high power microwave radiation with air, matter and plasmas have potential for various applications, and hence merit detailed studies and analysis. A detailed study, theoretical and experimental, is necessary in order to delineate possible regimes for applications purposes.

Studies can be performed analytically to provide answers in the limiting cases. However, the phenomena of the microwave interaction with air, matter and plasmas are complex and require time and space dependent treatments of a large number of physical processes. This can be carried out in a self consistent manner by developing detailed computer codes which treat part or all the phenomena.

This report deals with and describes computer codes, developed at NRL, for the analysis of the pulsed microwave interaction with nitrogen (N_2). The interaction is considered from the first principles with the microwave absorption by one or few free electrons, present in the gas, the electron build up, the breakdown, and the microwave absorption and reflection by the plasma electrons. The computer code which describes this phenomena is basically, consists of two codes coupled together. One, describes the electromagnetic radiation (E and M Code) and the other describes the physics and chemistry of the ionization and the deionization in N_2 (CHEM- N_2) Code. The E and M Code, however, can also be coupled into an air chemistry code to describe the breakdown in air, as discussed in the report.

In Section 1 the E and M Code and the solution of the wave equation is described. Section 2 gives the description of the pure N₂ chemistry code, and Section 3 deals with the breakdown calculations in N₂, where the breakdown power thresholds are compared with experimental data for several nitrogen pressures. In Section 4, the E and M Code coupled to an air chemistry code is utilized to calculate breakdown in air near a surface. For air breakdown near a surface one can utilize microwave powers below the threshold for air breakdown by a factor of 4 and still be able to break down the air. This is due to the fact that the microwave reflection from the surface interferes constructively with the outgoing wave resulting in doubling the electric field at a distance of $\frac{\lambda}{4}$ from the surface.

2. The E and M CODE

In order to describe the microwave absorption by a plasma one must know the electric field at all positions in the plasma. To do this we consider the solution of one dimensional wave equation¹

$$\frac{\partial^2 E_z}{\partial t^2} + \nu_c \frac{\omega_p^2}{\omega^2 + \nu_c^2} \frac{\partial E_z}{\partial t} - c^2 \frac{\partial^2 E_z}{\partial z^2} + \omega_p^2 \frac{\omega^2}{\omega^2 + \nu_c^2} E_z = 0 \quad (1)$$

for a plane wave incident normal to a plasma. The electron neutral (electron-ion) collision frequency is denoted by ν_c and the plasma frequency is defined as $\omega_p^2 = \frac{4\pi e^2 N_e}{m}$ where the notation is standard. Since the absorption length at microwave frequency is long at the critical density $N_c \equiv m \omega^2 / 4\pi e^2$ we can specify an essentially free-space boundary condition² for the incoming light as

$$\frac{\partial E_z}{\partial t} - c \frac{\partial E_z}{\partial y} = 2 \frac{\partial}{\partial t} U_{in} \quad (2)$$

where U_{in} is the amplitude of the known incident light. This boundary condition is also applicable to a plasma-vacuum interface as constructed in experiments using a mylar divider. The right side boundary condition in the plasmas specified as

$$\frac{\partial E_z}{\partial t} - c \frac{\partial E_z}{\partial y} = -4\pi j$$

where $j = \sigma E_z = \frac{v_c}{4\pi} \frac{\omega_p^2}{\omega^2 + v_c^2} E_z$. Again for low densities, the right hand side of equation (2) is similar to a free-space propagating to the right. Equation (1) is differenced implicitly to retain stability for large time steps in a high density plasma, $\omega_p^2 \geq v_c^2 + \omega^2$. The implicit difference form of equation (1) is

$$\frac{E_j^{n+1} - 2E_j^n + E_j^{n-1}}{(\Delta t)^2} + \frac{v_c}{2} \frac{\omega_p^2}{\omega^2 + v_c^2} \frac{E_j^{n+1} - E_j^{n-1}}{\Delta t} - \frac{c^2}{4} \frac{(\delta^2 E)_j^{n+1} + 2(\delta^2 E)_j^n + (\delta^2 E)_j^{n-1}}{(\Delta y)^2} + \omega_p^2 \frac{\omega^2}{\omega^2 + v_c^2} = 0 \quad (3)$$

where $(\delta^2 E)_j^n \equiv E_{j+1}^n - 2E_j^n + E_{j-1}^n$. This can also be cast into a tri-diagonal system of the form

$$\begin{aligned} -\beta^2 E_{j+1}^{n+1} + (1 + \gamma + 2\beta^2) E_j^{n+1} - \beta^2 E_{j-1}^{n+1} &= (2 - \omega_p^2 \Delta t^2 - 4\beta^2) E_j^n \\ + 2\beta^2 E_{j-1}^n + \beta^2 E_{j+1}^{n-1} - (1 - \gamma + 2\beta^2) E_j^{n-1} + \beta^2 E_{j-1}^{n-1} &= D_j^n \end{aligned} \quad (4)$$

where $\beta = \frac{\Delta t}{2\Delta y}$ and $\gamma = \frac{v_c}{2} \frac{\omega_p^2}{\omega^2 + v_c^2}$. A solution of a tri-diagonal

system of equations³

$$-A_j E_{j+1}^{n+1} + B_j E_j^{n+1} - C_j E_{j-1}^{n+1} = D_j^n$$

can be shown to be

$$E_{j+1}^{n+1} = G_{j+1}^{n+1} E_j^{n+1} + F_{j+1}^{n+1}$$

where the G_j 's and F_j 's satisfy the recursion relation

$$G_j^{n+1} = \frac{C_j}{B_j - A_j G_{j+1}^{n+1}} \quad \text{and} \quad F_j^{n+1} = \frac{D_j + A_j F_{j+1}^{n+1}}{B_j - A_j G_{j+1}^{n+1}} \quad (5)$$

The solution technique is then to specify the boundary condition and sweep the mesh space for the G_j 's and F_j 's. After which we sweep again to obtain the updated electric field.

The stability analysis of the implicit scheme can be made simple by dropping the last term of Equation (1). This term is typically not important in determining the stability criterion. We rewrite Equation (1) without this term as a system of two coupled equations.

$$\frac{\partial V}{\partial t} = v_c \frac{\omega_p^2}{\omega^2 + v_c^2} V + \frac{\partial W}{\partial y} \quad (6)$$

$$\frac{\partial W}{\partial t} = \frac{\partial V}{\partial y} \quad (7)$$

where $V = \frac{\partial E_z}{\partial t}$ and $W = \frac{\partial E_z}{\partial y}$. Choosing an arbitrary fourier

component we let $V_j^n = \xi^n \exp(-ik_j \Delta y)$ and $W_j^n = \rho^n \exp(-ik_j \Delta y)$.

We find after some algebra that

$$\begin{pmatrix} \xi \\ \rho \end{pmatrix}^{n+1} = \frac{1}{1 + \alpha^2 + \gamma^2} \begin{pmatrix} 1 - \gamma - \alpha^2 & 2i\alpha \\ 2i\alpha & 1 + \gamma - \alpha^2 \end{pmatrix} \begin{pmatrix} \xi \\ \rho \end{pmatrix}^n = A \begin{pmatrix} \xi \\ \rho \end{pmatrix}^n \quad (8)$$

where $\alpha = \frac{c \Delta t \sin(k \Delta y / 2)}{\Delta y}$. Stability requires the eigenvalues of the amplification matrix A to be less than or equal to 1. One can show that the eigenvalues are bounded by

$$|\lambda^{\pm}| = \frac{1 - \gamma + \alpha^2}{1 + \gamma + \alpha^2} \leq 1 \quad (9)$$

and hence the implicit scheme is unconditionally stable for arbitrary α .

The boundary conditions are explicitly differenced and are coupled to an explicit form of Equation (1) to obtain boundary value. This explicit form of Equation (1) is:

$$\frac{E_j^{n+1} - 2E_j^n + E_j^{n-1}}{(\Delta t)^2} + \frac{v_c}{2} \frac{\omega_p^2}{\omega^2 + v_c^2} \frac{E_j^{n+1} - E_j^{n-1}}{\Delta t} - c^2 \frac{E_{j+1}^n - 2E_j^n + E_{j-1}^n}{(\Delta y)^2} + \omega_p^2 \frac{\omega^2}{\omega^2 + v_c^2} E_j^n = 0 \quad (10)$$

Once the boundary values are obtained, we use the implicit difference equation for all interior points. The boundary values are used as "first" values in sweeping the tri-diagonal system of equation. Since locally the explicit differencing is stable for

$$(\Delta t)^2 \left[\left(\frac{c}{\Delta y} \right)^2 + \frac{1}{4} \left(v_c \frac{\omega_p^2}{\omega^2 + v_c^2} \right)^2 \right] \leq 1$$

the boundary must be at low density to maintain stability, $\omega_p^2 \leq v_c^2 + \omega^2$.

In practice, the implicit scheme must satisfy the explicit stability criterion to maintain accuracy and minimum phase error. In considering microwave breakdown off a reflecting surface, this is important since the interference maximum determines the breakdown field.

As a check on the code, we perform simulations, on free-space, propagation and reflection off metal surface in a vacuum. Figure (1a) shows the reflected light for a propagating electromagnetic wave in vacuum for a single pass to the reflecting surface and back to the point of entry of the radiation. The system length is $kL = 15$ (where $k = 2\pi/\lambda$) so the return time of the radiation is $t_{R,W} = 30$ for $c\Delta t = 0.9\Delta y$. The code tracks the propagation velocity well, however, in the transient time $\omega t \leq 30$, the numerics has introduced errors in the reflected wave. The average reflected wave should be zero during the transient period, yet we see the average reflected wave of roughly 10% of the incident light. Figure (1b) shows the spatial electric field (in normalized variables). Since the launched incoming wave is unity, the combined wave once reflected from the surface should be of amplitude two. We see the implicit scheme has introduced large errors in the phase of the wave and therefore the reconstructed wave. Figure (2a) shows a similar test with a reduced time step $c\Delta t = 0.2\Delta y$. However, in this test, the reflected wave in the transient period is less than 1% of the incident light. The smaller phase error reconstructs the interference patterns to its proper maximum of two as can be seen in Figure (2b). An extensive parameter study shows good results are obtained using the implicit scheme for $c\Delta t \leq 0.2\Delta y$.

Also as a check, we consider light normally incident on a linear density profile. The density profile in this collisionless plasma ($\nu_c = 0.1\omega$) rises from zero to the cut off density N_c with a density scale length of $kL_s = 10$. The Airy function solution requires standing wave pattern toward the incident light and evanescent wave in the overdense plasma. Figure (3) shows the solution obtained for the electric field using the implicit scheme with the boundary conditions. Analytic solution shows the computed field is accurate in location of the first large maximum, the amplitude of the reflected light and the amplitude of the largest maximum. The various test problems thus confirm the validity of the code.

3. N₂ BREAKDOWN AND OPTICAL DIAGNOSTICS

To describe the nitrogen breakdown by the microwave radiation, we have

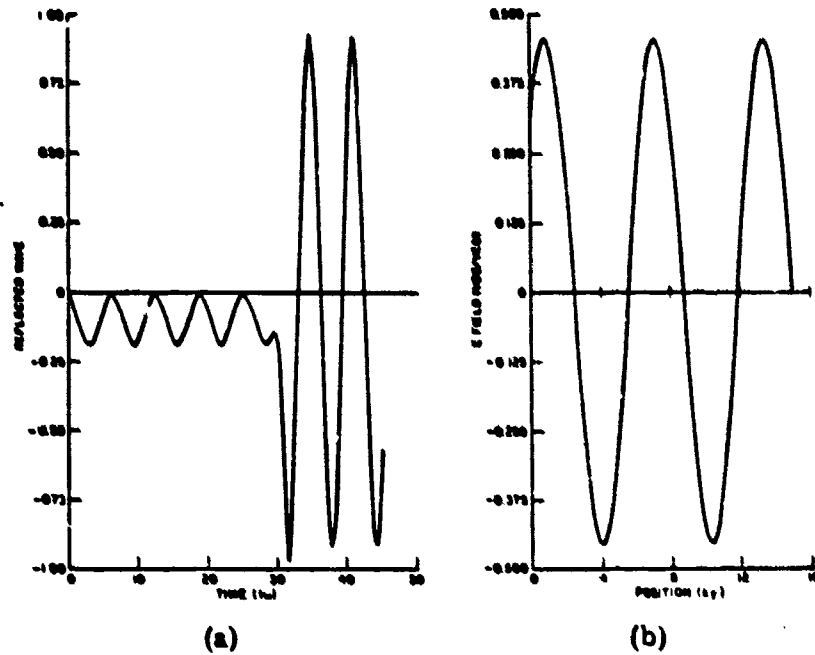


Fig. 1 — Test run with $c\Delta t = 0.9\Delta y$ for a plane wave reflected from a surface (a) reflected wave (VOS/VEO) versus time ($t\omega$) and (b) electric field (VOS/VEO) versus position (ky) where VOS and VEO indicate the oscillatory and the thermal velocities of the electron, respectively.

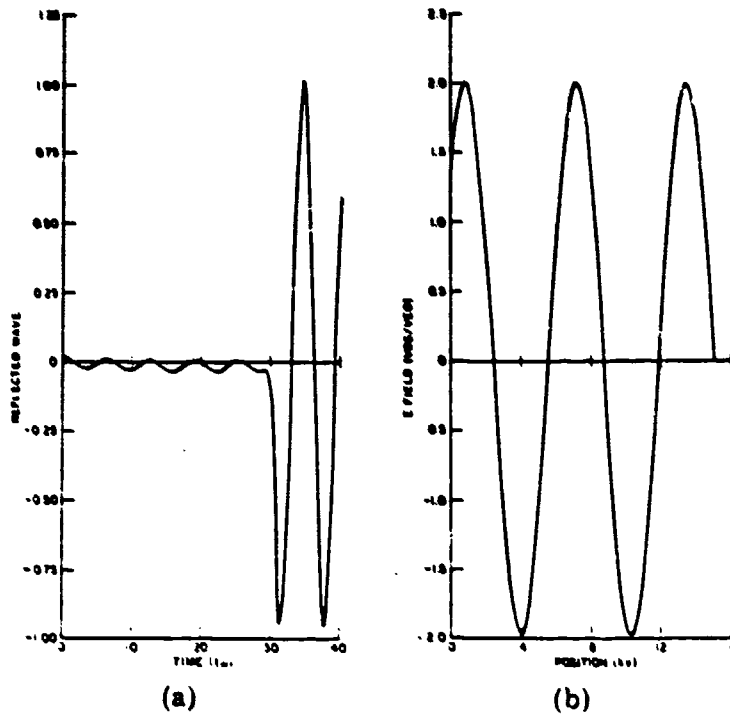
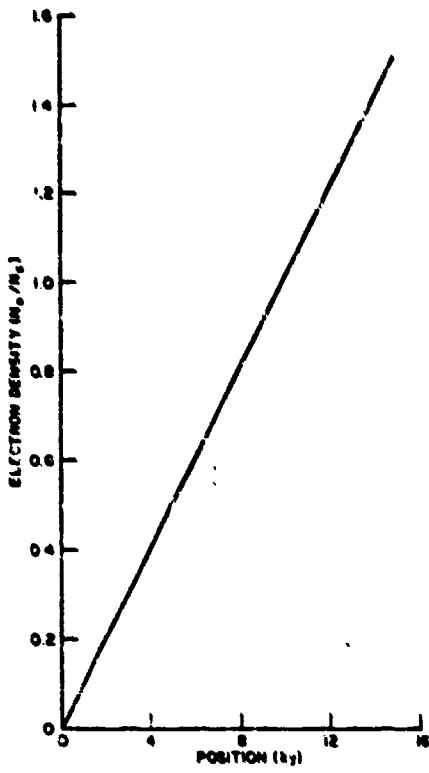
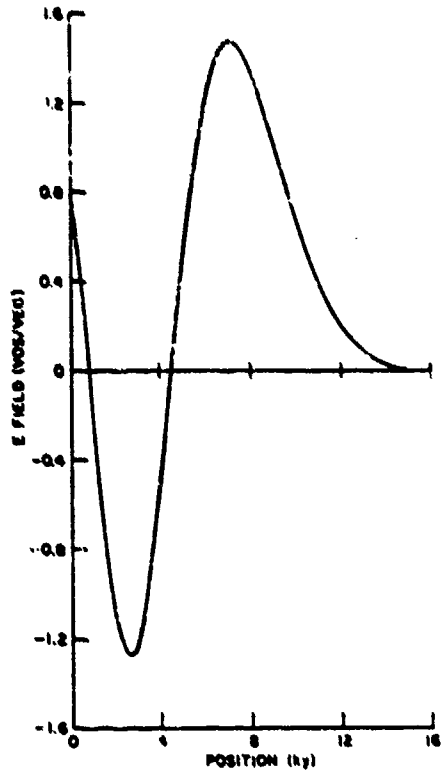


Fig. 2 — Test run with $c\Delta t = 0.2\Delta y$ for a plane wave reflected from a surface (a) reflected wave (VOS/VEO) versus time ($t\omega$) and (b) electric field (VOS/VEO) versus position (ky) where VOS and VEO indicate the oscillatory and the thermal velocities of the electron, respectively.



(a)



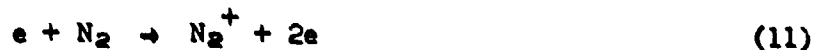
(b)

Fig. 3 — Test run for a plane wave normally incident on a linear plasma profile. The graph shows the electric field (VOS/VE₀) versus position (ky).

developed an N_2 chemistry code. The code calculates the time developments of $N_2^+(x)$, $N_2^+(B)$, N_4^+ , N , $N(^2D)$, $N_2(A^3\Sigma)$, $N_2(B^3\Pi)$, $N_2(C^3\Pi)$, N_e , T_e , T_v , and T_g , where the last three symbols designate the electron, the N_2 - vibrational and the gas temperatures, respectively. The purpose for the calculation of the population densities of several excited states is to provide volume emission rates for optical diagnostics of the plasma and the investigation of the ionization from the excited states.

3.1 N_2 CHEMISTRY

A free electron gains energy, in the field of the microwave radiation, it undergoes both elastic and inelastic collisions with N_2 , thereby losing part or all of the energy gained from the field. When the electron energy reaches and overshoots the ionization threshold for N_2 an ionization event may occur according to reaction (11).

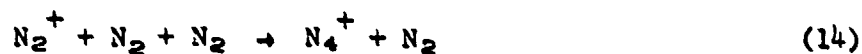


Higher energy electrons could ionize N through the dissociative ionization. However, the threshold for this process is higher by ~ 10 eV compared to that for reaction (11). Therefore, process (11) is the predominant reaction for the breakdown ionization by microwave radiation.

The deionization of the plasma occurs primarily through the dissociative recombination of the nitrogen ion N_2^+ and its cluster ion N_4^+ , i.e.,



The N_4^+ cluster forms via a three-body process^{4,5} i.e.,



and is obviously important at atmospheric pressures and lower gas temperatures. When the gas temperature rises, however, the formation of N_4^+ is inhibited by the slowing down of the forward reaction in (14) and by the collisional breakup of N_4^+ (i.e., the reverse reaction of (14) becomes operative.

The deionization also proceeds via the three-body collisional recombination, however, it may become important after breakdown and when the electron density is quite high. Finally, the electron loss occurs also through diffusion.

3.2 ELECTRON ENERGY GAIN AND LOSS PROCESSES IN N₂

The electron energy loss processes in N₂ proceed by the elastic and inelastic collisions. The energy loss by elastic collisions is dependent on ν_c , where ν_c is the momentum transfer collision frequency. The collision frequency depends on the electron energy (temperature) and the momentum transfer cross section. The cross section⁶ is shown as a function of the electron energy in Figure (4). By folding this cross section with the appropriate electron velocity distribution, one obtains the momentum transfer collision frequency. Thus the rate of the energy loss by an electron through the elastic collisions can be expressed as

$$R_e = \frac{2m}{M} \nu_c \left(\frac{3}{2} T_e - \frac{3}{2} T_g \right) \quad (15)$$

where m is the electron mass and M is the mass of the nitrogen molecule.

The electron inelastic energy loss processes in N₂ are the excitation, the dissociation and the ionization of the nitrogen molecule. These processes are expressed as



in addition to Equation (1). Equation (16) indicates the excitations of the N₂ ground state vibrational levels, while Equation (17) represents the excitations of the electronic states of N₂. The N₂ electronic states include the triplets and the singlets whose cross sections are presented and discussed elsewhere.⁷ The cross section for the N₂ disassociation, however, is a composite of a large number of singlet states which predissociate. Thus, the energy loss by electrons in N₂ can be summed up to include the losses due to the excitations of the ground state vibrational levels, the excitation of

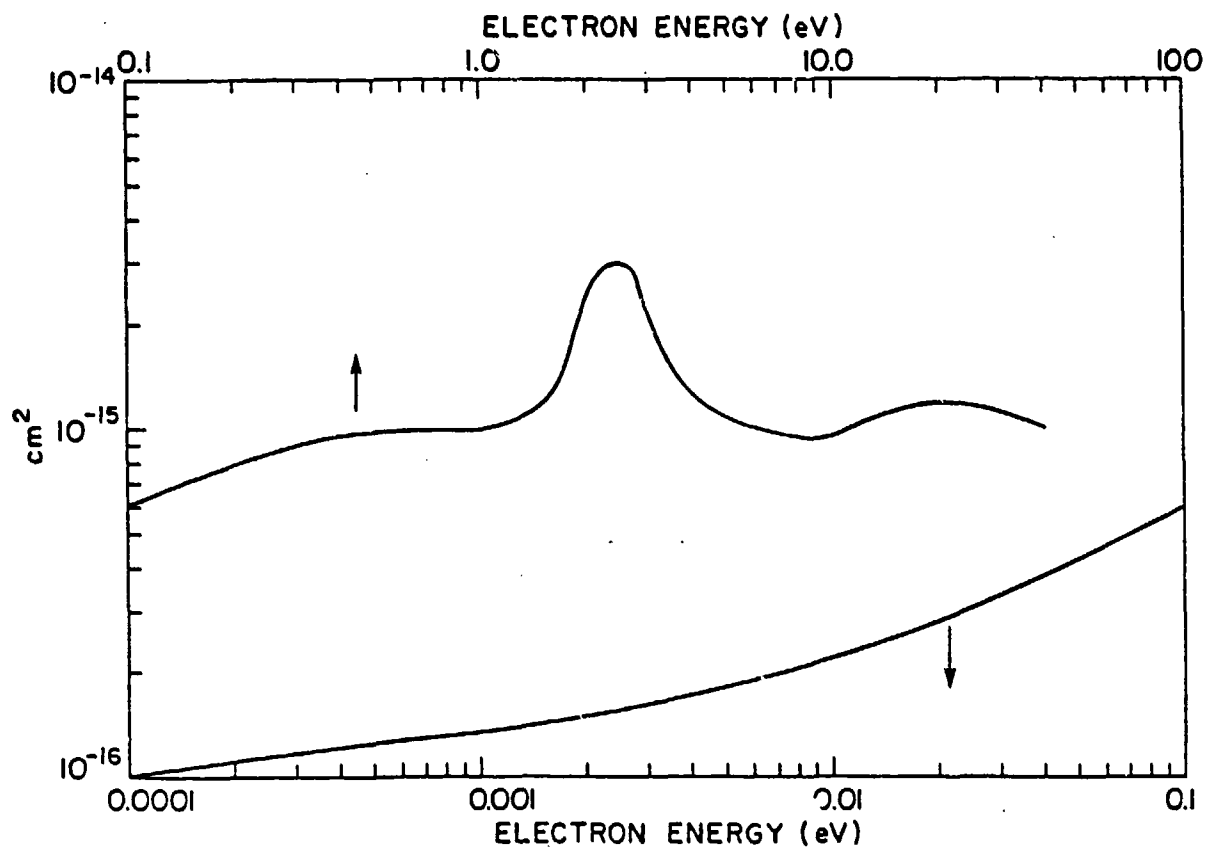


Fig. 4 - The Electron Momentum Transfer cross section in nitrogen (N₂)

the electronic states A^2_ϵ , B^3_ϵ , C^3_π , a^1_π , the dissociation, and the ionization of N_2 .

Briefly, the vibrational cross sections are from the measurements of Schulz⁸ and are well established as to the peak of the total and the shape of the individual cross sections⁸⁻¹⁰. The cross section for the ionization is from the measurement of Rapp and Golden¹¹ and the cross section for the dissociation is from the measurements of Winters¹² and Zipf and McLaughlin¹³. The cross section for the triplet states are discussed in the next section.

The rate coefficients for all the inelastic processes discussed above have been obtained^{14, 15} for a Maxwellian electron velocity distribution and are utilized in the breakdown code. Thus, if one designates x_i as the electron impact rate-coefficient for the excitation of the i th state whose excitation energy is E_i , the rate of the electron energy loss in N_2 can be expressed as

$$R_{in} = \sum_i x_i E_i N_2$$

Where the summation is over eight ground state vibrational levels, the singlet and triplet electronic states, the dissociation and the ionization of N_2 . A similar equation for the energy loss in the nitrogen atom can be utilized, with the appropriate rate coefficients.

Other electron energy loss processes are the excitation of the excited states from a lower state (not the ground state) and the ionization of the excited states.

The energy gain mechanisms for an electron are the energy absorption from the field of the microwave i.e., the inverse bremsstrahlung, the electron impact deexcitation of the ground state vibrational levels and the deexcitation of the electronic states of the N_2 molecule and the nitrogen atom.

3.3 EXCITED STATES

The code as indicated earlier calculates the time histories of several excited states of N_2 which are discussed below.

A^3_Σ : The A^3_Σ state is a metastable and has a life time of 1 sec and an

excitation¹⁶ energy of 6.1 eV. Its excitation cross section by electron impact has been measured and calculated by several investigators which are discussed in Ref (7), and shown in Figure 5. The electron impact ionization of the A³Σ state has been calculated by Kukulin, et al.¹⁷ The excitation energy of the A³Σ state generally ends up as a heating source for the gas because of the rapid quenching of the state by the atomic nitrogen. The rate coefficient for the quenching¹⁸ of the A³Σ by N is 5×10^{-11} cm³/sec.

B³Σ: The B³Σ state is excited, from the ground state of N₂, by electron impact, has an excitation energy¹⁶ of 7.2 eV, and is the upper level for the first positive band system, (B³π → A³π). The strong vibrational bands of this system¹⁸ are given in Table 1.

B³π

TABLE 1

Relatively Strong Emissions in the First Positive Band System

Wave length (Å)	Transition (v, v')	Wavelength (Å)	Transition (v, v')
7503	4, 2	6069	6, 2
6704	5, 2	6013	7, 3
6623	6, 3	5959	8, 4
6544	7, 4	5906	9, 5
6468	8, 5	5854	10, 6
6394	9, 6	5804	11, 7
6322	10, 7	5755	12, 8

The life times of these transitions are in the range of 10^{-5} sec to 10^{-6} sec and are quenched¹⁹ by N₂ with a rate coefficient of $\sim (1-2) \times 10^{-11}$ cm³/sec.

The electron impact excitation cross section for the B³π state have been measured and calculated by numerous investigators⁷ and some of these are shown in Figure 6.

C³π: The C³π state is excited from the ground state of N₂, by electron impact has an excitation energy¹⁶ of 11 eV and is the upper level for the second positive band systems, (C³π → B³π). Some of the strong¹⁸ bands of this system are given in Table 2.

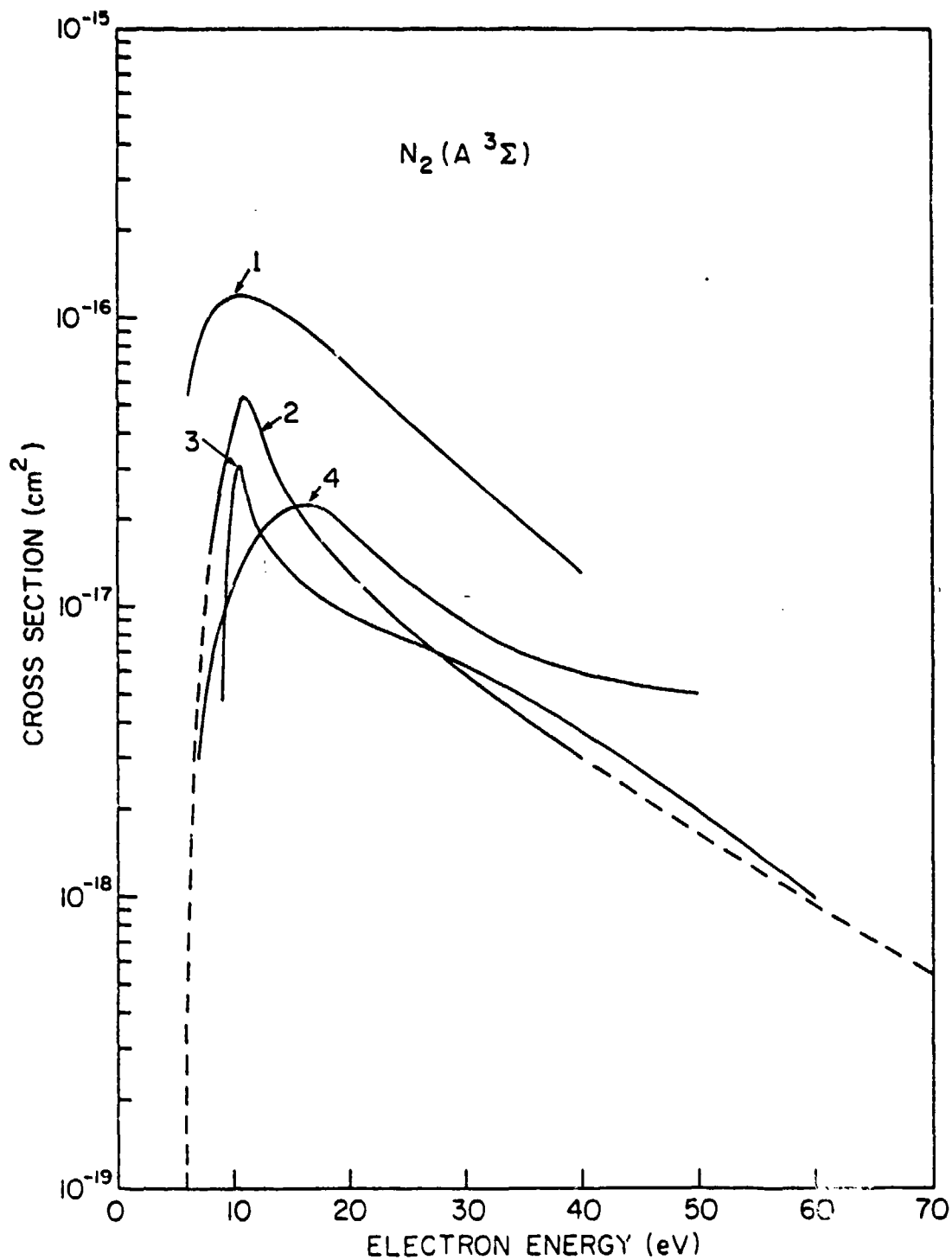


Fig. 5 — The Electron Impact Excitation Cross Section of $N_2(A^3\Sigma)$. For details see Ref. (7).

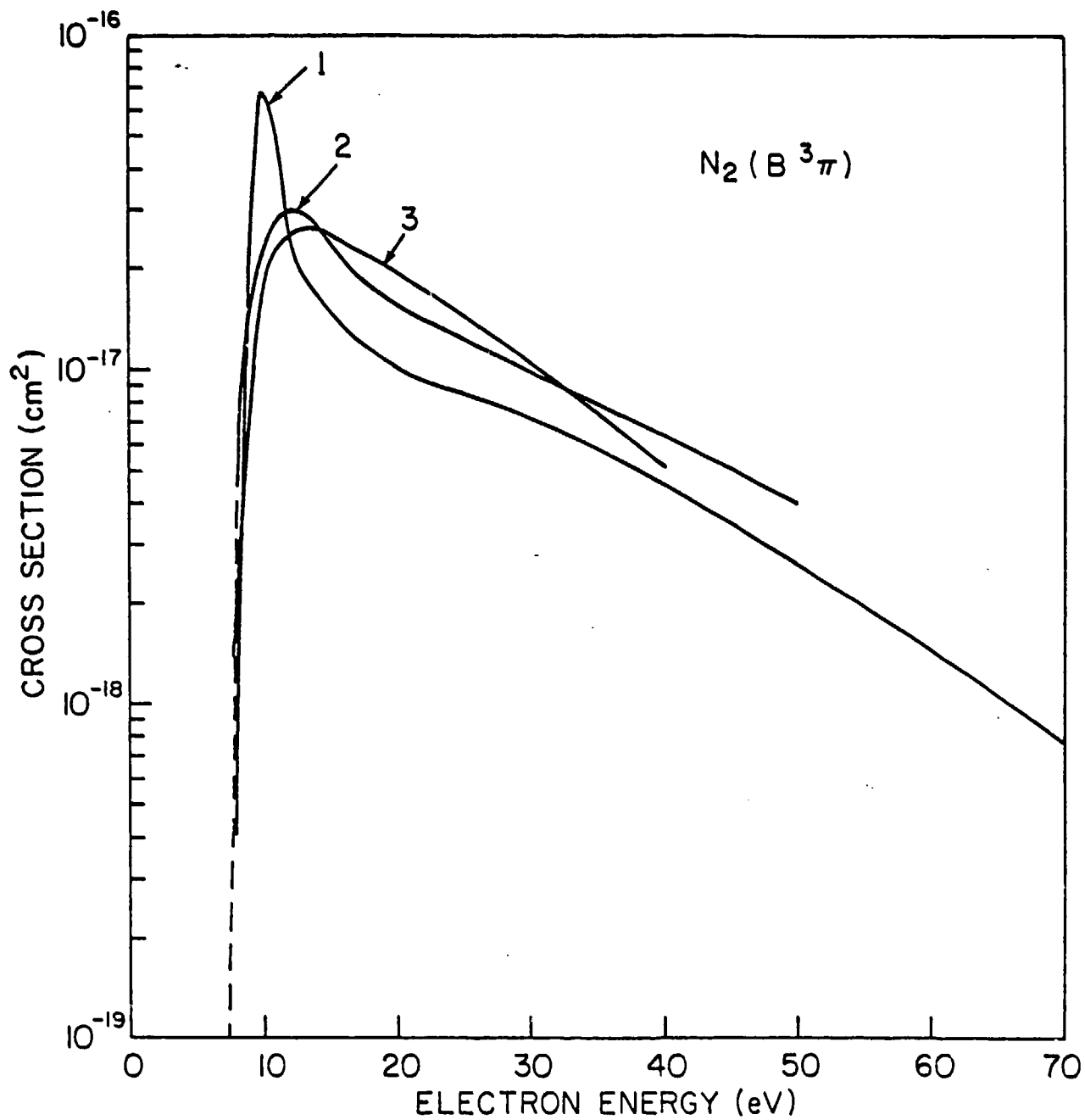


Fig. 6 — The Electron Impact Excitation Cross Section of $N_2(B^3\Pi)$. For details see Ref. (7).

TABLE 2

Relatively Strong Emissions in the Second Positive Band System

<u>Wavelength (\AA)</u>	<u>Transition (ψ, ψ')</u>	<u>Wavelength (\AA)</u>	<u>Transition (ψ, ψ')</u>
4059	0, 3	3755	1, 3
3998	1, 4	3710	2, 4
3943	2, 5	3577	0, 1
3894	3, 6	3536	1, 2
3804	0, 2	3371	0, 0
		3159	1, 0
		3163	2, 1

The lifetimes of these transitions are²⁰ in the range of tens of nanoseconds to fractions of a microsecond. Those vibrational levels are quenched by N_2 where the rate coefficient for the quenching of the (0, 0) transition is²¹ $1.15 \times 10^{-11} \text{ cm}^3/\text{sec}$.

The electron impact excitation cross section for the second positive band system has been calculated and measured extensively,⁷ especially the cross section for the excitation of the (0, 0) transition at 3371 \AA . The excitation cross section is shown in Figure 7.

$N_2^+(B)$: The nitrogen molecule has several ionization continua where upon the ionization the molecular ion is in an excited state. These are $N_2^+(A)$, $N_2^+(B)$, $N_2^+(C)$, etc. The $N_2^+(B)$ state has an ionization threshold of 13.3 eV and is the upper level for the first negative band system, $N_2^+(B^2\Sigma \rightarrow X^2\Sigma)$. The strong^{1B} emissions from this band system are given in Table 3.

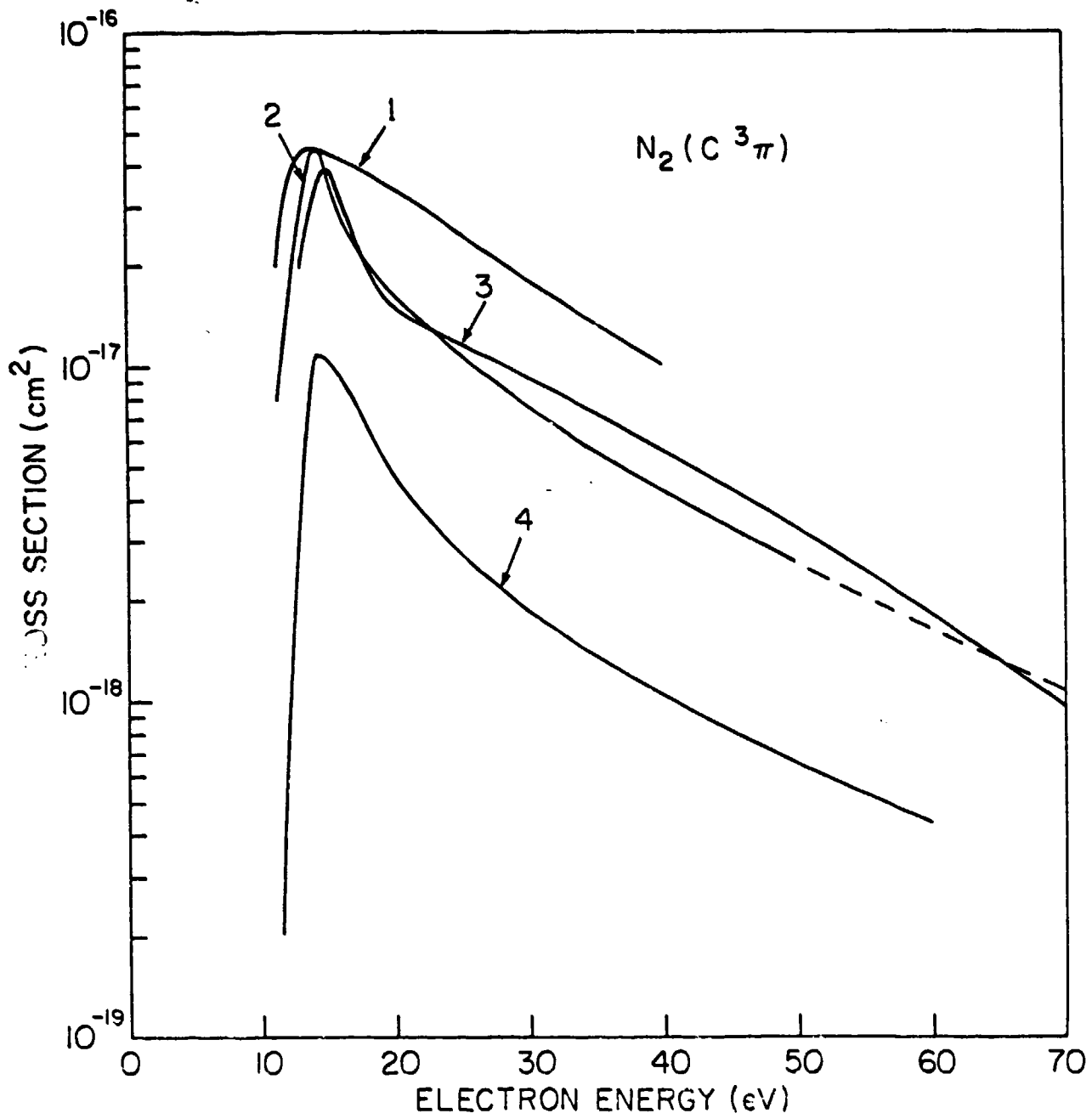


Fig. 7 — The Electron Impact Excitation Cross Section of $N_2(C^3\Pi)$. For details see Ref. (7).

TABLE 3

Relatively Strong Emissions in the First Negative Band System

Wavelength (Å)	Transition (v, v')	Wavelength (Å)	Transition (v, v')
5228	0, 3	4236	(1, 2)
5076	2, 5	3914	(0, 0)
4709	0, 2		
4599	2, 4		
4515	4, 6		
4278	0, 1		

The lifetimes of these states range²⁰ from tens of nanoseconds to microseconds and are quenched rapidly by N₂. The rate coefficient²² for the quenching of the zeroth vibrational level is 4×10^{-10} cm³/sec.

The fractional ionization leading to the N₂⁺(B) state is well established⁷ for ionization by electrons with energy of 100 eV and higher. However, some data exist²³ for the fractional ionization below 100 eV, and emission cross section²⁴ which should be of more relevance to the ionization of N₂ by the microwave radiation.

N(²D): The metastable state of the nitrogen atom has an excitation energy¹⁵ of 2.37 eV and arises by the dissociation of N₂, the dissociative recombination of N₂⁺, and by direct electron impact excitation from the ground state of N. The electron impact excitation cross section of N(²D) has been calculated.⁷

3.4 GAS HEATING

One of the basic interests in the air breakdown is the heating of the plasma and the neutral species. The heating of the neutral species and the ions (since the collision between heavy particles is very efficient we assume that the ions and the neutrals have the same temperature) occurs through several atomic and molecular processes. These are: the elastic collisions of the electrons with the heavy particles, the quenching of the excited electronic states by the neutral species, the dissociative recombination of the molecular ions and the charge exchange process. The quenching of the vibrational energy through the collision between neutral species and vibrationally excited molecules is another essential source for the heating of the gas. However, the slowest heating rate among these various processes is the vibrational - translational energy exchange.

When the gas temperature rises, two additional ionization processes become operative. These are the thermal ionization and the associative ionization as expressed by Equations (20) and (21), respectively.



4. APPLICATIONS TO BREAKDOWN STUDIES

There exist considerable experimental^{25,26} data on the microwave breakdown in air and other gaseous elements. With the advent of lasers, the air breakdown studies at optical frequencies have increased considerably.²⁷⁻²⁹ Theoretical calculations for the air, or gas breakdown generally proceed from the Boltzman's equation which is solved self consistently for the electron energy and its distribution. Analytical methods^{26,27,30} are also utilized to obtain the breakdown threshold power. In this report we have assumed a maxwellian electron velocity distribution in our codes (we are planning to develop a Boltzman code for this purpose) and have utilized the code for the breakdown calculations.

4.1 MICROWAVE BREAKDOWN IN N_2

In order to compare our results with experiments, we have incorporated the effect of diffusion into the code. Thus we define an effective ionization rate $\nu_{ei} = \nu_i - D \Lambda^{-2}$ to allow for diffusion in our code. The diffusion is assumed to be free with a diffusion coefficient $D = V_e^2 t_c^2 \approx 5 \times 10^{15} T_e$. The time $t_c = 1/\nu_c$ is the electron-neutral (electron-ion) collision time and V_e is the electron thermal velocity. The diffusion length Λ is regarded as being specified by the cavity and is assumed known. Our definition of breakdown is defined as the electric field required to achieve a net increase in the electron density for a ten nanosecond pulse. Once the cascade process begins, the electron density quickly reaches the critical density. The dominant loss processes at low and high pressures ($P \geq 1$ Torr) are diffusion and dissociative recombination ($N_4^+ + e \rightarrow N_2 + N_2$), respectively. Our comparison will be to experimentally measure cw breakdown in nitrogen. The criterion for cw breakdown in nitrogen is $\nu_i = \nu_r + D/\Lambda^2$ where ν_r is the dissociative recombination rate³¹, $\nu_r = 5.0 \times 10^{-9} N_4^+/T_e$, where T_e is in eV. Both the diffusion length Λ and the ambient electron density ($n_0 = 10^{22} \text{ cm}^{-3}$) were specified in the experiment and are known parameters in our calculation.

Calculations were performed for various frequencies, diffusion lengths, and pressures. Figure (8) shows the results obtained by MacDonald et al.²⁰ for cw breakdown fields in nitrogen at frequencies 992MH and 9.4GH with diffusion lengths of 0.631 cm and 0.4 cm, respectively. The stars in Figure (8) denote the calculated breakdown threshold intensity using N₂-Chem. The calculated thresholds are higher as expected for pulsed breakdown. Table 4 shows the electron temperature, breakdown intensity, and characteristic time for electron production $\tau = N_e (dN_e/dt)^{-1}$ as a function of the background pressure at $f = 922$ MH and $\Lambda = 0.631$ cm.

Table 4

Pulse Breakdown Threshold Power for 10 cm Wavelength for Various Nitrogen Pressures

<u>Neutral density (cm⁻³)</u>	<u>Electron Temperature (eV)</u>	<u>Pulse Breakdown Power (Watts/cm²)</u>	<u>τ (sec)</u>
1.32 x 10 ¹⁸	1.7	2200.	7.1 x 10 ⁻⁷
1.32 x 10 ¹⁷	2.4	80.	4.3 x 10 ⁻⁷
1.32 x 10 ¹⁶	6.4	60.	2.5 x 10 ⁻⁷
1.32 x 10 ¹⁵	41.0	153.	3.7 x 10 ⁻⁸

The characteristic time τ represents roughly the maximum growth time for the electrons at the start of the avalanche process. Experiments show that once the pulse length $t_p \geq 25\mu s$, the pulse breakdown threshold approaches the cw breakdown limit. The generation time is approximately $t_g = \tau \log 2$ and we require 20 - 25 generations to reach electron densities of order $N_e \sim 10^{11} \text{ cm}^{-3}$. Again our definition of the breakdown power is the intensity required to achieve a net increase in the electron density in 10 ns. Therefore, our results are certainly applicable to pulse breakdown when $t_g \ll 25\mu s$. Since this is easily satisfied by our results, we would expect the higher breakdown field as characteristic of pulse breakdown. The high electron temperature at low pressure results from the strong diffusive losses. The agreement at lower pressures may be somewhat fortuitous since we extrapolate the ionization and excitation rates to energies above 20 eV. Current rate coefficients in the code are tabulated for T_e up to 20 eV.

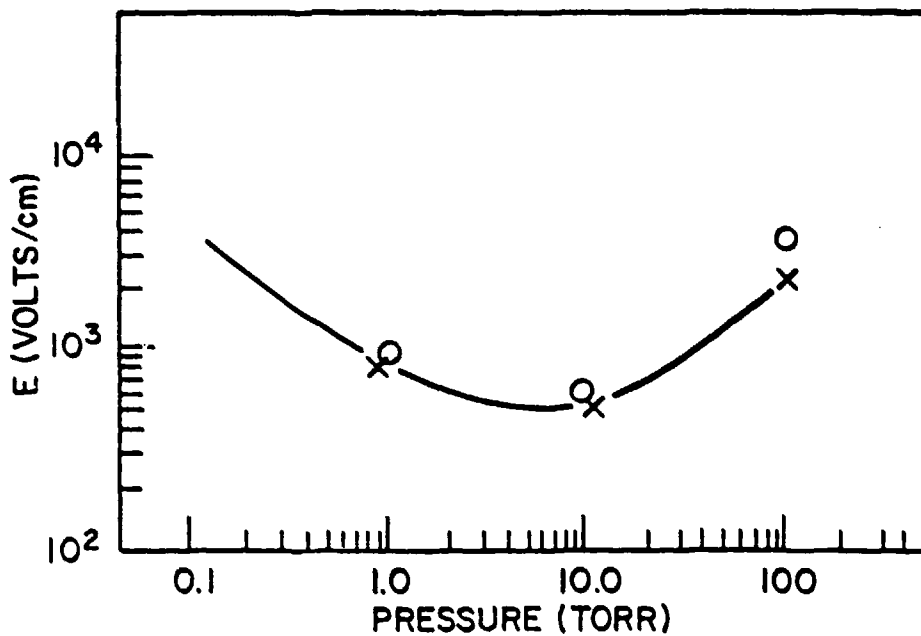
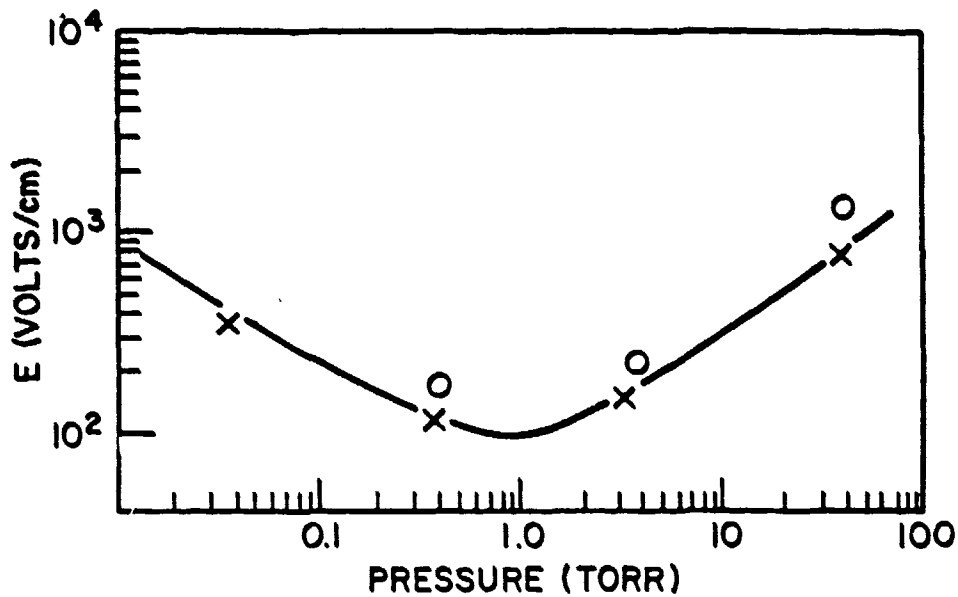


Fig. 8 - Comparison between experimental CW N₂ breakdown threshold power and calculations using the N₂ chemistry code, CHEMN2. Calculations are indicated by circles and crosses for pulsed and CW breakdown fields, respectively.

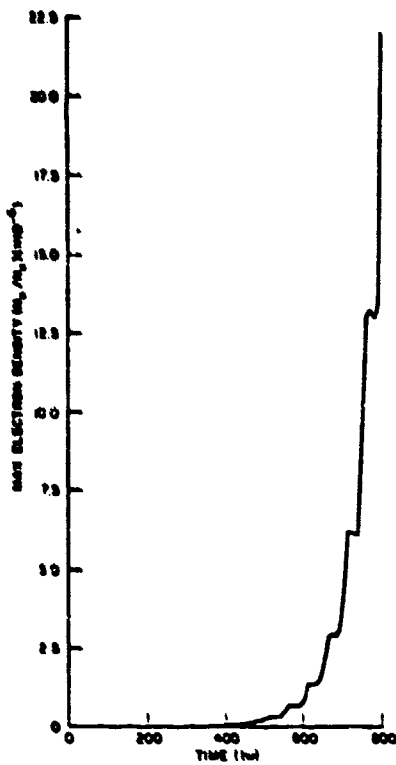
However, data is available for T_e above this temperature and will be incorporated into the code if desired.

4.2 MICROWAVE AIR BREAKDOWN OFF A REFLECTING SURFACE

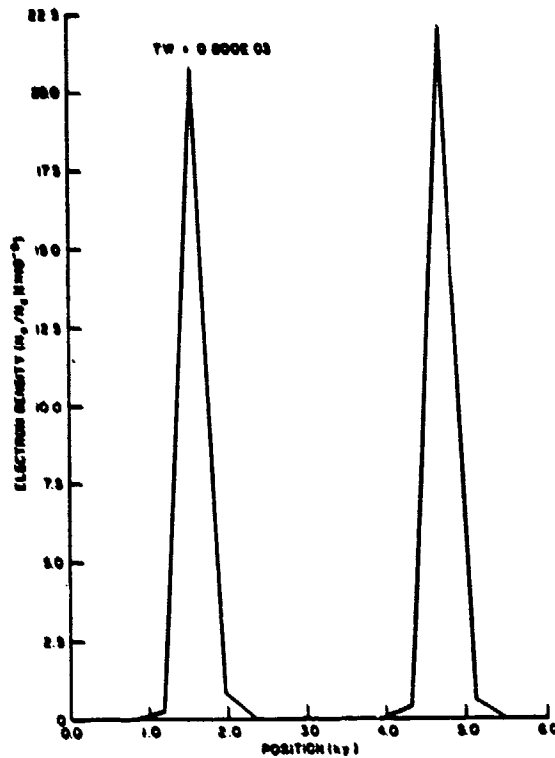
We have also coupled the E and M code to a detailed air chemistry code³² (CHMAIR) to study the breakdown in air. We have, however, chosen to calculate the breakdown off a reflecting surface to illustrate the breakdown in air as a result of the interference between the incident and the reflected waves. In these calculations we neglect the hydrodynamic effects and assume that chemical processes are more effective in depleting the electron density than diffusion. This is especially true in microwave absorption experiments with short pulses ($t_p \leq 40$ ns) and rather long wavelength radiation conducted at atmospheric pressures. Assuming the diffusion length $\Lambda = \lambda$, at atmospheric condition the characteristic electron diffusion time, for 10 cm radiation, is roughly $t_D = (\Lambda/L_{mfp})^2 t_c = 10^{-7}$ sec where L_{mfp} is the mean free path of the electron. Since the diffusion time $t_D \gg t_p = 40$ ns, our neglect of hydrodynamic effect would seem a good assumption.

The intensity of the standing wave patterns resulting from the interference maximum can easily be above the threshold for air breakdown. We imagine the microwave to be incident on a reflecting surface with intensity $I_0 < I_B$. At the first maximum (one-quarter wavelength from the surface) the field intensity is $I = 4 I_0$ with air breakdown commencing rapidly a distance $\frac{\lambda}{4}$ from the surface (Figure 9a). Figure 9b shows the rapid increase of the electron density as the avalanche begins. The extreme sensitivity of the air breakdown to the electric field essentially localizes the electron density resulting in sharp scale lengths, $L = N_e (dN_e/dy)^{-1} < \lambda$. In this simulation, we have a pulse of 10cm wavelength radiation incident normal to a reflecting surface with an intensity of $I_0 = 0.5$ MW/cm² and a pulse duration of 40ns. The initial ambient electron density is taken to be $n_0 = 10$ cm⁻³ at standard temperature and pressure (STP).

In a collisional plasma, $\nu_c \gg \omega$, the cut off density for propagation of electromagnetic radiation is not sharply defined as in collisionless plasmas. At sufficiently high density such that the skin depth $\delta \leq \lambda$, the breakdown region closest to the surface is decoupled from the microwave radiation. This is seen in Figure 10a, where we show the square of the electric field at the end of a 40ns pulse. In this particular simulation, we allow for multiple sources (each source below threshold) such that the net intensity

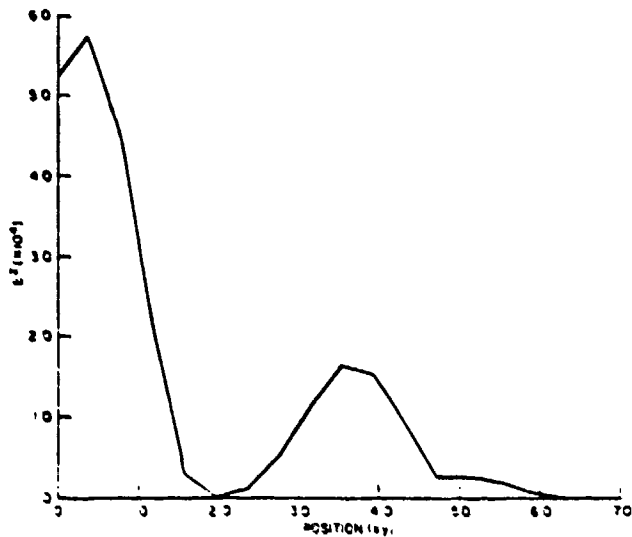


(a)

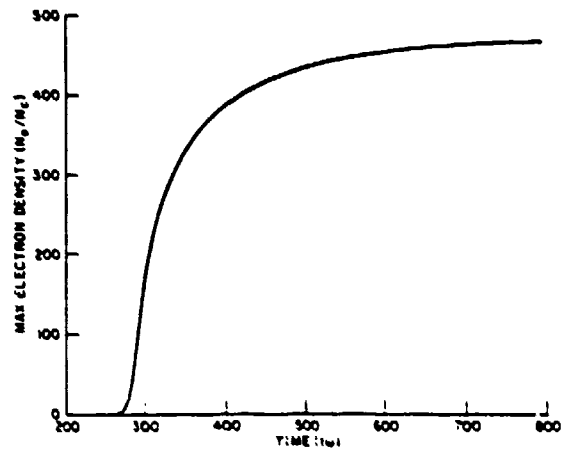


(b)

Fig. 9 — (a) Air breakdown off a reflecting surface at atmospheric conditions with incident power $I = 0.5 \text{ MW/cm}^2$ at $\lambda = 10 \text{ cm}$. (b) Time development of the electron density (N_e/N_c).



(a)



(b)

Fig. 10 — (a) The square of the electric field at the end of the pulse for $t_p = 40 \text{ nsec}$. (b) Time development of the electron density (N_e/N_c).

$I_0 = 2\text{MW}/\text{cm}^2 > I_B$. The corresponding density for $\delta < \lambda$ can be easily calculated to be $N_e \approx 500N_c$. Figure 10b shows the time history of the rise of the electron density to $N_e \approx 500N_c$. Though air breakdown is occurring throughout the volume for this particular simulation, the extreme sensitivity of the air breakdown to the electric field again localizes the region of the electron density. The important point to be made here is the high electron density. As will be shown later, the reflection coefficient for an idealized sharp electron density profile is insignificant until $N_e \approx 10^5 N_c$ at $\lambda = 10\text{cm}$. The high electron density makes real the possibility of driving a hydrodynamic response with microwaves, pending the inclusion of the hydrodynamic effects and various pulse shapes and pulse lengths. Early work by Wood³³ using the hydrodynamic code LASNEX suggests the formation of shocks at atmospheric conditions using microwave radiation.

4.3 REFLECTION OF MICROWAVE RADIATION

Once the electron density becomes sufficiently large $N_e \gg N_c$, the plasma becomes a good absorber of microwave radiation. However, at too high densities, the plasma becomes a good reflector of microwave. We wish to obtain maximum bounds on the reflection and absorption coefficient of the plasma as a function of wavelength and electron density. We proceed further by calculating the absorption and reflection coefficient for an idealized slab density profile of density N and thickness d (See Figure 11). We consider multiple reflection and vary the wavelength, density, and thickness of the microwave plasma system. In particular we examine the reflection at two microwave frequency of 3GH and 30GH, respectively. The electron-neutral collision frequency is assumed to be $\nu_c = 5 \times 10^{12} \text{sec}^{-1}$ which is typical at ambient atmospheric conditions. The reflection and transmission coefficients are given by

$$R = \left| \frac{E_{\text{ref}}}{E_{\text{inc}}} \right|^2 = \left| \frac{S (1 - e^{-i\epsilon})}{1 - S^2 e^{-i\epsilon}} \right|^2$$

and

$$T = \left| \frac{E_{\text{Trans}}}{E_{\text{inc}}} \right|^2 = \left| \frac{(1 - S^2) e^{-i\epsilon/2}}{1 - S^2 e^{-i\epsilon}} \right|^2$$

SIMPLE PHYSICAL MODEL

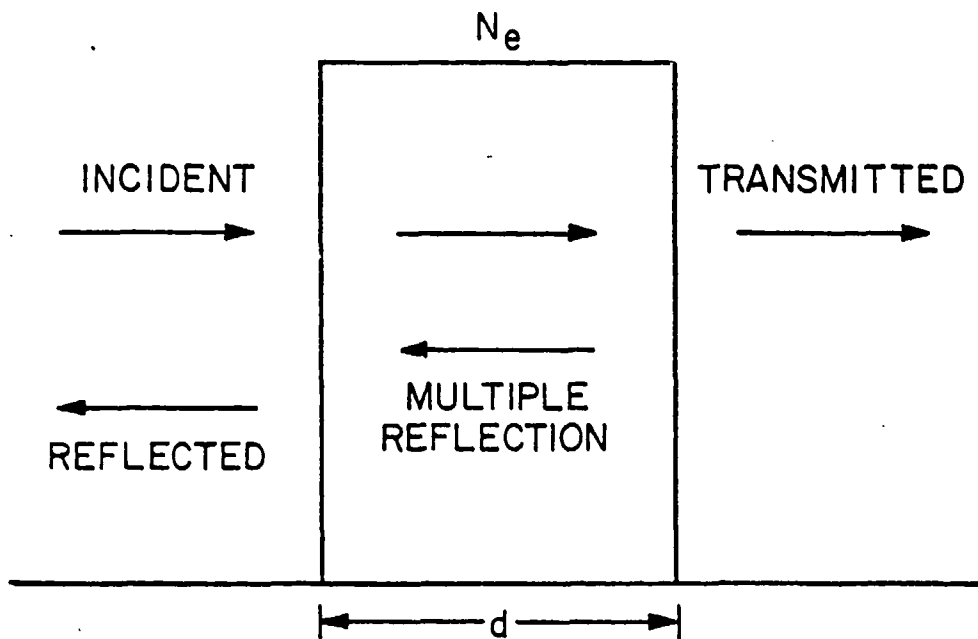


Fig. 11 — The idealized slab density profile is characteristic of systems with high electron densities and steep density profiles.

where $S = (1 - n)/(1 + n)$ and $\epsilon = 2n\omega d/c$. The complex refractive index

$n = n_r - in_i$ is

$$n_r = \left\{ \frac{(1 - a)}{2} \left[1 + \sqrt{1 + \frac{4b^2}{(1 - a)^2}} \right] \right\}^{\frac{1}{2}}$$

$$n_i = \left\{ \frac{(1 - a)}{2} \left[1 + \sqrt{1 + \frac{4b^2}{(1 - a)^2}} \right] \right\}^{\frac{1}{2}}$$

when $1 - a > 0$ and

$$n_r = \left\{ \frac{(a - 1)}{2} \left[\sqrt{1 + \frac{4b^2}{(a - 1)^2}} - 1 \right] \right\}^{\frac{1}{2}}$$

$$n_i = \left\{ \frac{(a - 1)}{2} \left[\sqrt{1 + \frac{4b^2}{(a - 1)^2}} + 1 \right] \right\}^{\frac{1}{2}}$$

when $1 - a < 0$, where $a = \frac{\omega_p^2}{(\omega^2 + \nu_c^2)}$ and $b = \frac{\nu_c a}{2\omega}$.

The absorption is determined by the condition $R + T + A = 1$ with the thickness measured in units of the skin depth δ , $\delta k = \frac{1}{n_i}$. Since the results for $d = \delta$ and $d \gg \delta$ are somewhat similar, we present the results only for $d \gg \delta$.

Figure 12 shows the reflection and absorption coefficients, as a function of plasma density at $\lambda = 10\text{cm}$ and $\lambda = 1\text{cm}$ light, respectively. If we assume an absolute electron density of $N_e = 10^{15}\text{cm}^{-3}$, we see the reflection coefficient is roughly 60% for 10cm light ($N_e = 10^4 N_c$). Whereas, for 1cm light, the reflection coefficient is approximately 25% at $N_e = 10^{15}\text{cm}^{-3} = 10^2 N_c$. Our calculations also indicate that to maintain a plasma density of $N_e = 10^{15}\text{cm}^{-3}$ requires an absorbed power of $I_{\text{abs}} \approx 0.3\text{MW/cm}^2$. Using a 10cm light would require an incident power level of $I_{\text{inc}} \geq 1.6\text{MW/cm}^2 > I_B$. Obviously, once the incident power is above the breakdown threshold, the

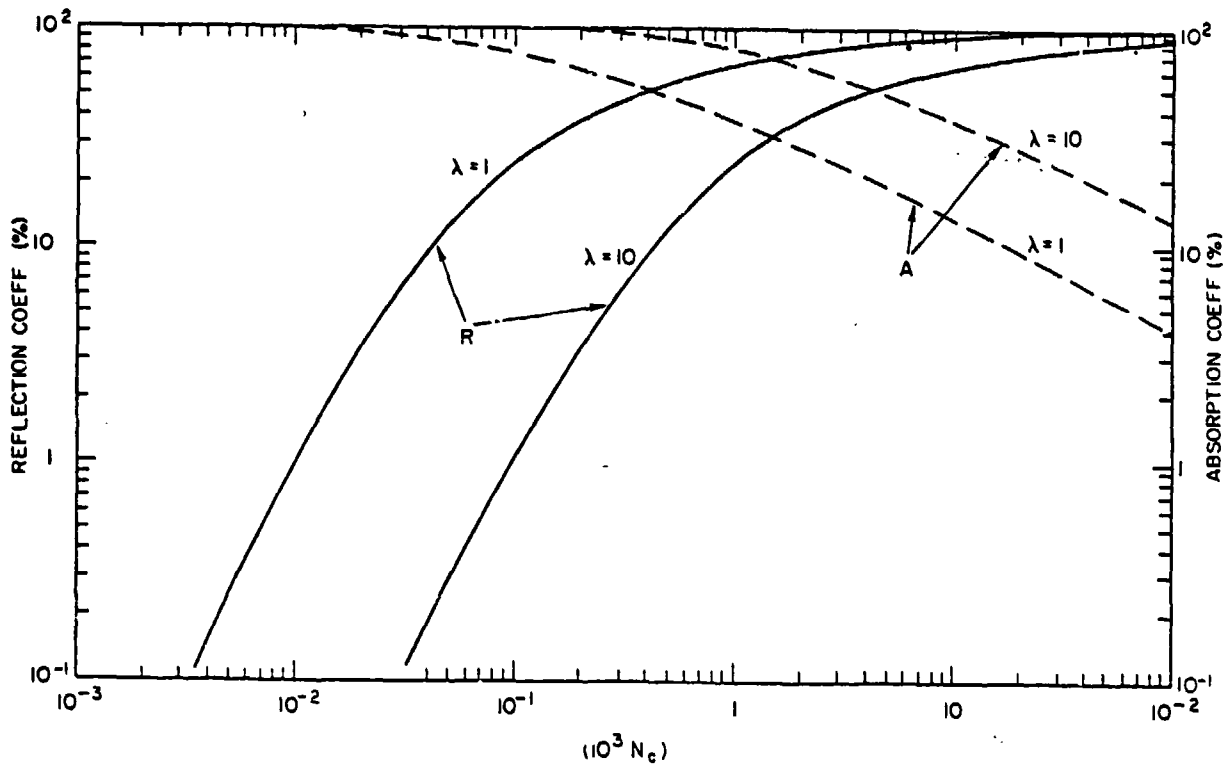


Fig. 12 — Reflection and absorption coefficient as a function of the electron density in the slab plasma model with $\nu_c = 5 \times 10^{12} \text{ sec}^{-1}$.

plasma would be impossible to maintain. However, the prospects of maintaining a plasma at $N_e = 10^{15} \text{cm}^{-3}$ using a 1cm light appears feasible since an incident intensity of $I_{inc} \approx 1 \text{MW/cm}^2 < I_B$ would only be required. Though the electron density $N_e = 10^{15} \text{cm}^{-3}$ is clearly arbitrary, it is not unreasonable to expect the plasma to become a good reflector when

$$\omega_p^2 \geq \nu_c^2 + \omega^2.$$

5. Conclusions

We have presented and discussed two codes developed for the studies of the pulsed microwave interaction with N_2 . We have also utilized our E and M code coupled to a chemistry code to study the breakdown in air. Our breakdown threshold power calculations agree favorably with experimental data in N_2 .

Our calculations for breakdown near a surface brings forth the importance of reflection from a plasma on its maintenance and heating. However, additional studies in this subject are in progress to delineate this point further, including the hydrodynamic effects.

REFERENCES

1. V. L. Ginzburg, "Propagation of Electromagnetic Waves in Plasma", Pergamon Press, Oxford (1964).
2. E. L. Lindman, J. Computational Phys. 18, 66 (1975).
3. R. D. Richtmyer and K. W. Morton, "Difference Method for Initial Value Problems", J. Wiley, New York (1967).
4. R. N. Varney, Phys. Rev. 89, 708 (1953), *ibid* 174, 165 (1968) and references therein.
5. J. L. McCrumb and P. Warneck, J. Chem. Phys. 66, 5416 (1977).
6. A. G. Englehardt, A. V. Phelps and C. G. Risk, Phys. Rev. 135, A1566 (1964).
7. A. W. Ali, "Excitation and Ionization Cross Sections for Electron and Microwave Energy Depositions in Air", NRL Memo Report 4598 (1981).
8. G. J. Schultz, Phys. Rev. 135, A988 (1964) and references therein.
9. D. Spence, J. L. Maurer and G. J. Schulz, J. Chem. Phys. 57, 5516 (1972).
10. H. Eherhard and K. Willman, Zeit, Phy. 204, 462 (1967).
11. D. Rapp and P. Englander-Golden, J. Chem. Phys. 43, 1464 (1965).
12. H. F. Winters, J. Chem. Phys. 44, 1472 (1966).
13. E. C. Zipf and R. W. McLaughlin, Planet Space Sci. 26, 449 (1978).
14. A. W. Ali, "The Physics and the Chemistry of Two NRL Codes for the Disturbed E and F Regions", NRL Report 7578 (1973).
15. A. W. Ali, "The Physics and the Chemistry of NRL Master Code for the Disturbed E and F Regions", NRL Memo Report 3732 (1978).
16. A. W. Ali, R. H. Kummler, F. R. Gilmore and J. William McGowan, "Upper Atmospheric Excitation Processes", NRL Memorandum Report 3920 (1979).
17. V. I. Kuklin, A. P. Osipov and Y. M. Chuvilskii, Soviet Physics, Tech. Phys. 24, 883 (1980).
18. R. W. B. Pearse and A. G. Gaydon, "The Identification of Molecular Spectra", Chapman and Hall, London (1965).
19. D. C. Cartwright, J. Geophys. Res. 83, 517 (1978).
20. R. W. Nicholls, Annals de Geophys. 20, 144 (1964).
21. P. Millet, Y. Salamero, H. Brunet, J. Galy, D. Blanc and J. L. Teyssier, J. Chem. Phys. 58, 5839 (1973).
22. M. N. Hirsh, E. Poss and P. N. Eisner, Phys. Rev. A1, 1615 (1970) and references therein.

23. G. R. Wight, M. J. Van der Wiel and C. E. Brion J. Phys. B. Atom. Mol. Phys. 9, 675 (1976).
24. J. W. McConkey, J. M. Woolsey and D. J. Burns, Planet Space Sci. 15, 1332 (1967).
25. M. A. Herlin, and S. C. Brown, Phys. Rev. 74, 291 (1948).
26. A. D. MacDonald, D. V. Gaskell and H. N. Gitterman, Phys. Rev. 130, 1841 (1963).
27. See e.g. C. Demichelis, IEEE, J. Quantum. Electron, QE-5, 188 (1969) and references therein.
28. N. Krall and K Watson, Phys. Rev. A5, 1883 (1972).
29. Y. P. Raizer, "Laser-Induced Discharge Phenomena", Consultants Bureau, New York (1977).
30. A. W. Ali, "The Microwave Application Theory Program at NRL and Some Chemistry Code Applications to Ionospheric Heating by Microwave Radiation", NRL Memo Report 4302 (1980).
31. M. A. Biondi, Chapter 16, Defense Nuclear Agency Reaction Rate Handbook, DNA 1948 H., Bortner and Baurer Eds., DASIAC, DoD Nuclear Information and Analysis Center, GE-Temp, Santa Barbor, Ca. (1972).
32. R. F. Fernsler, A. W. Ali, J. R. Greig and I. M. Vitkovitsky, NRL Memo Report 4110 (1979).
33. C. H. Wood, Bull Am Phys. Sci 25, 909 (1980).

APPENDIX B

Microwave Energy Coupling in a Nitrogen Breakdown Plasma

C. L. Yee, A. W. Ali†, and W. M. Bollen

Naval Research Laboratory, Washington, D. C. 20375

ABSTRACT

Computer simulations of microwave coupling to a nitrogen breakdown plasma have been performed at 25 Torr. Non-hydrodynamic ionization fronts are observed to propagate toward the radiation source under a variety of circumstances. Free nitrogen breakdown simulations in a spherical system show the propagation velocity of the breakdown wave can be as high as 5×10^6 cm/sec. An elementary theory is used for estimating the speed of the breakdown wave in one dimension. The results are in reasonable agreement with breakdown experiments.

† Plasma Division, Naval Research Laboratory.

1.0 Introduction

The pulsed breakdown in air and other gaseous elements has been studied extensively¹ with emphasis on the threshold power for breakdown and its dependence on the gas pressure and radiation wavelength. The hydrodynamic effects were first considered by Lin and Theofilos.² Their calculation of the gas heating showed that both high field intensity above the breakdown intensity and increasing molecular density discouraged energy deposition in air. Though the preliminary experimental results confirmed the general features of the simple theory, the observed pressure waves were stronger than predicted. Scharfman³ et al., have observed that a breakdown plasma prevents the transmission of microwave energy to points beyond the plasma. Experiments⁴ recently performed at the Naval Research Laboratory (NRL) showed that the microwaves are rapidly decoupled from a target or plasma surface. This rapid decoupling of the microwaves would limit the amount of energy that can be deposited into the gas. Computer simulations of the NRL experiments have been performed at a pressure of 25 Torr in nitrogen. Throughout this work, we have used the MINI code developed at NRL to help in understanding the basic interaction processes in the experiments.

2.0 The Microwave Nitrogen Interaction Code (MINI)

The Microwave Nitrogen Interaction code (MINI) used in our studies is an one-dimensional multi-species, multi-temperature, hydrodynamic, nitrogen chemistry and wave optics code. The species followed dynamically were N_2 , $N_2^+(X)$, $N_2^+(B)$, N_4^+ , N , $N(^2D)$, $N_2(A^3\Sigma)$, $N_2(B^3\Pi)$, $N_2(C^3\Pi)$, and the electron density (n_e). The model calculates the electron (T_e), vibrational (T_v) and gas (T_g) temperatures, and is space and time dependent with microwave absorption and reflection considered in the wave optics mode. The detail of the chemistry and the wave optics aspect of the code are described elsewhere⁵ and will not be

repeated here. The electrons are described hydrodynamically by the equations

$$\partial_t (n_e) + \nabla \cdot (n_e \vec{u}_e) = C_e$$

$$\vec{u}_e = \vec{u}_m - \mu_e \vec{E} - D_e \nabla (\ln n_e) - D_e \nabla (\ln T_e)$$

$$\partial_t (\epsilon_e) + \nabla \cdot \{ \epsilon_e \vec{u}_e + p_e \vec{u}_e + \vec{Q}_e \} = \vec{R}_e \cdot \vec{u}_e + \vec{J}_e \cdot \vec{E} + E_e$$

$$\epsilon_e = \frac{3}{2} n_e T_e + \frac{1}{2} m_e n_e u_e^2$$

where $p_e = n_e T_e$ is the electron pressure, $\vec{J}_e = -en_e \vec{u}_e$ is the electron current density, $\vec{R}_e = -m_e n_e \nu_c (\vec{u}_e - \vec{u}_m)$ is the electron momentum transfer rate, $\mu_e = e/m_e \nu_c$ is the electron mobility, and $D_e = T_e/m_e \nu_c$ is the electron diffusion coefficient. The electron momentum transfer frequency is ν_c , and m_e is the mass of the electron. The electron energy flux is $\vec{Q}_e = -\kappa_e \nabla T_e$ where the electron thermal conductivity is $\kappa_e = \beta n_e T_e / m_e \nu_c$ and β is a constant. The terms on the right hand side of the energy equation represent energy lost due to heat flow, work due to momentum transfer, joule heating and heating due to elastic, inelastic, and chemical processes. The term C_e represents sources and sinks terms for the electron due to ionization, recombination, and attachment. The E_e term in the electron energy equation includes energy losses due to vibrational and electronic excitation of molecular nitrogen. The C_e and E_e terms are discussed more fully in Ref. (5). The average velocity of molecular nitrogen, \vec{u}_m , is related to the diffusion and mass-average-velocity⁶ of the heavy particles by $\vec{u}_m = \vec{v}_m + \vec{u}$. The diffusion velocity is \vec{v}_m , and \vec{u} is the mass-average-velocity of the heavy particles.

The continuity equation for each of the heavy particle species is

$$\partial_t(n_i) + \vec{\nabla} \cdot (n_i \vec{u}_i) = C_i.$$

The momentum equation for the heavy particles is

$$\partial_t(\rho \vec{u}) + \vec{\nabla} \cdot (\rho \vec{u} \vec{u} + \underline{\Pi}) = \rho^+ \vec{E} - \vec{R}_e$$

where $\rho = \sum_i m_i n_i$, $\rho^+ = \sum_i Z_i e n_i$, and $\underline{\Pi} = \underline{\pi} + p_H \underline{I}$ are the mass density, positive charge density, and pressure tensor. The viscous portion of the pressure tensor is $\underline{\pi}$, $p_H = T_g \sum_i n_i$ is the heavy particle pressure, and \underline{I} is the unit tensor. The heavy particle energy equation is

$$\partial_t(\epsilon_H) + \vec{\nabla} \cdot \{\epsilon_H \vec{u} + \vec{Q}_H + \underline{\Pi} \cdot \vec{u}\} = -\vec{J}_e \cdot \vec{E} + \vec{R}_e \cdot \vec{u}_e + \frac{n}{\tau_v} m \{\epsilon_v(T_v) - \epsilon_v(T_g)\} + E_H$$

$$\epsilon_H = \sum_i c_i n_i T_g + \frac{1}{2} \rho u^2$$

where ϵ_H is the total energy density, c_i is the translation-rotational specific heat, $\epsilon_v(T_v) = \epsilon \{\exp(\epsilon/T_v) - 1\}^{-1}$ is the average vibrational energy per molecule,⁷ $\epsilon = 0.3$ eV is the quantum of vibrational energy for nitrogen, τ_v is the characteristic time for vibrational relaxation,⁸ and E_H is the heating terms due to chemical, elastic, and inelastic processes. Again a more detailed discussion of E_H can be found in Ref. (5). The heavy particle energy flux is $\vec{Q}_H = -\kappa_H \vec{\nabla} T_g$, and κ_H is the thermal conductivity of the gas, including translational and rotational contribution.⁹ The average and diffusion velocity of species i are related by $\vec{u}_i = \vec{v}_i + \vec{u}$. The diffusion velocity of the i th ion species is \vec{v}_i and \vec{u} is the mass-average-velocity of the heavy particles

$$\vec{u} = \frac{1}{\rho} \sum_i m_i n_i \vec{u}_i = \vec{u}_m.$$

The vibrational energy equation may be written approximately as

$$\partial_t \{n_m \epsilon_v(T_v)\} + \vec{\nabla} \cdot \{n_m \epsilon_v(T_v) \vec{u}_m + \vec{Q}_v\} = - \frac{n_m}{\tau_v} \{ \epsilon_v(T_v) - \epsilon_v(T_g) \} + E_v$$

where $\vec{Q}_v = -\kappa_v \vec{\nabla} T_v$ is the vibrational energy flux and κ_v is the vibrational conductivity. The vibrational temperature can be calculated assuming that the nitrogen molecule is a harmonic oscillator and that the vibrational levels have a Boltzman distribution. Hence, the vibrational energy source term E_v is

$$E_v = \epsilon n_m n_e \{1 - \exp(-\epsilon/T_v)\} \sum_{v=1}^8 v X_v \{1 - \exp[\epsilon v(T_v - T_e)/T_v T_e]\}$$

where X_v is the excitation rate coefficient¹⁰ for the vth vibrational level obtained from the experimentally measured cross-sections.¹¹ The vibrational energy spacing is $\epsilon = 0.3$ eV for nitrogen.

The equations solved in MINI are:

$$\partial_t (n_e) + \partial_x (n_e u_e) = C_e \quad (1)$$

$$u_e = u_m - \mu_e E - D_e \partial_x (1 n n_e) - D_e \partial_x (1 n T_e) \quad (2)$$

$$\partial_t (\epsilon_e) + \partial_x \{ \epsilon_e u_e + p_e u_e + Q_e \} = R_e u_e + J_e E + E_e \quad (3)$$

$$\epsilon_e = \frac{3}{2} n_e T_e + \frac{1}{2} m_e n_e u_e^2$$

$$\partial_t (n_i) + \partial_x (n_i u_i) = C_i \quad (4)$$

$$\partial_t (\rho u) + \partial_x \{ \rho u^2 + p_H - (\frac{4}{3} \mu + \mu_B) \partial_x u \} = \rho^+ E - R_e \quad (5)$$

$$\partial_t (\epsilon_H) + \partial_x \{ \epsilon_H u + \{ p_H - (\frac{4}{3} \mu + \mu_B) \partial_x u \} u + Q_H \} \quad (6)$$

$$= \frac{n_m}{\tau_v} \{ \epsilon_v(T_v) - \epsilon_v(T_g) \} - J_e E - R_e u_e + E_H$$

$$\partial_t \{n_m \epsilon_v(T_v)\} + \partial_x \{n_m \epsilon_v(T_v)u\} = - \frac{n_m}{T_v} \{\epsilon_v(T_v) - \epsilon_v(T_g)\} + E_v \quad (7)$$

where the Kinematic and bulk viscosity coefficients are μ and μ_B . The transport coefficients for the viscosity and thermal conductivity are taken from Bird.¹²

The dc portion of the electric field and the diffusion velocities are determined by demanding the total current

$$\vec{J}_T = \vec{J}_e + \sum_i \vec{J}_i = 0 \quad (8)$$

where $\vec{J}_i = Z_i e n_i \vec{u}_i$ is the current density of the i th ion species.

In steady state, each of the ion species satisfies an equation

$$\vec{u}_i = \vec{u}_m + \mu_i \vec{E} - D_i \vec{\nabla}(\ln n_i) - D_i \vec{\nabla}(\ln T_g) \quad (9)$$

where the ion diffusion coefficient and mobility are related to the collision frequency ν_i by $D_i = T_g/m_i \nu_i$ and $\mu_i = Z_i e/m_i \nu_i$.

The mass of the i th ion species is m_i . Summing Eq. (9) for all ion species and using Eq. (8) gives an equation for the ambipolar electric field. Once the ambipolar field is found, Eqs. (9) and (2) are used to solve for the flow velocities of the ions and the electron.

The Eulerian difference equations of Eqs. (1) - (7) are solved using the algorithm of Rubin and Burstein.¹³ The scheme is simple, second order in accuracy, and is relatively stable while centering the dissipation terms. The hydrodynamic and chemistry portions are calculated separately in a cycle, assuming the flow velocities of the fluid are weak. The hydrodynamics is determined from the updated values of the chemistry. Hence, the hydrodynamics is considered as a small correction to the chemistry.

3.0 Cascade Ionization of Nitrogen by a Microwave Pulse

Microwave gas breakdown begins when a small number of priming electrons acquire sufficient energy from the electric field to ionize the gas. These priming electrons gain energy when the oscillatory energy of the electrons in the electric field is randomized by collisions into thermal energy. Once an electron has an energy in excess of the ionization energy of the gas, the electron can easily ionize the gas, resulting in the generation of two low energy electrons. The electron avalanche can be described by

$$n_e(t) = n_e(0)\exp(t/\tau_B) \quad (10)$$

where $n_e(t)$ is the electron density at time t , and τ_B is the breakdown time. Physically, τ_B is the time required for an electron to gain the energy needed to ionize the gas.¹⁴ Fig. 1 shows the breakdown time, τ_B (sec), and the electron temperature, T_e (eV), for conditions typical of microwave breakdown of N_2 . A high radiation field would promote the electron avalanche by increasing the energy imparted to the electron per collision with the molecule. A high molecular density, however, requires higher intensities for the avalanche breakdown. At moderate pressures above 25 Torr, the dominant energy loss mechanism for the electrons is the excitation of the electronic and vibrational modes of the gas. The root-mean-square electric field to density ratio, E/n_m ($V\text{-cm}^2$), does not uniquely define the absorbed energy for an ac electric field. The striped region in Fig. 1 is bounded by the constant intensity line (I) and the constant pressure line (P). The rapid variation in τ_B with increasing intensity allows a breakdown threshold, I_B , to be assigned at the onset of breakdown. The ability to couple microwave energy to a breakdown gas depends sensitively on the breakdown time, τ_B , and the electron density.

The efficiency of converting microwave energy to the translational energy of the gas can be enhanced by coupling the microwaves to a preformed plasma. Plasma maintenance of a preformed plasma by microwaves allows the microwave deposition to be localized while maintaining a high electron density. In short pulse breakdown experiments with pulse lengths, $\tau_p < 1 \mu\text{sec}$, a high electron density is a necessary condition for rapid heating of the gas. Plasma maintenance requires the breakdown time $\tau_B > \tau_p$ when $n_e(0) \gg 1$. If the local electric field is not carefully matched to the instantaneous plasma conditions, the gas heating will be self-limited by the formation of a non-hydrodynamic ionization front. Gas breakdown off a reflecting surface without a preformed plasma will not result in a local deposition of the microwave energy. Since the microwave deposition is determined self-consistently with the electron density profile, the resulting plasma density cannot rapidly heat the gas in the short pulse experiments.

3.1 Gas Breakdown Near a Reflecting Surface

A plane wave incident normal to a reflecting surface would require less power for gas breakdown. The constructive interference of the incident and reflected microwave results in the characteristic standing wave pattern for the electric field and a factor of four increase in the field intensity. If the intensity is above the breakdown threshold, breakdown of the gas occurs instantaneously at the peak nodes of the electric field. As the electron density rises, these "pancakes" of electrons begin to attenuate the radiation. Pancakes closest to the reflecting surface rise more rapidly early in the pulse (Fig. 2). As the electron density continues to rise, attenuation of the microwave causes the pancakes closest to the surface to fall in density below that of pancakes far from the surface. Shorter systems with fewer pancakes decouple more rapidly than longer systems. However, the total absorbed energy remains essentially constant, independent of the system size for a fixed pressure and pulse length.¹⁵

The finite length simulations represent the planar region near the surface of a focused microwave system where the distance from the surface is less than the radius of the spotsize. Fig. 2 shows two similar simulations with $I = 6.25 \text{ kW/cm}^2$ for an one-and-a-half and three wavelength system without hydrodynamic effects. The plasma absorbs approximately 20% of the total microwave energy with an asymptotic absorption efficiency of 80%. The absorption is regulated by the electron density. Shorter systems have a much higher electron density than larger systems and can more readily heat the gas in the short pulse experiments. The gas is not expected to be heated more than the observed 4% above the ambient temperature in a weakly focused system. The absorbed energy is distributed over a larger number of pancakes with a very low electron density. As will be discussed later, the low electron density of Fig. 2 results in a long heating time for the gas of $\tau_g \approx 6.5 \text{ } \mu\text{sec}$ where $\tau_g \equiv T_g(dT_g/dt)^{-1}$. The time required to heat the gas to an appreciable temperature in a weakly focused system would require pulse lengths of $\tau_p > 6.5 \text{ } \mu\text{sec}$. However, even for long pulses, a significant heating of the gas is never realized. Later in the pulse, the pancakes furthest away from the reflecting surface continue to rise in density. Ultimately, a single pancake will have sufficient density to reflect the radiation. This pancake acts as a secondary reflecting surface and decouples the radiation from the primary metallic surface. Gas breakdown experiments⁴ using a reflecting surface show this behavior. Similarly, free nitrogen breakdown simulations without a surface using a focused system also show that the radiation is decoupled from the initial breakdown site.

3.2 Maintenance of a Preformed Plasma by Microwaves

Microwave coupling to a pre-ionized plasma near a metallic surface show some general characteristics. Though the plasma absorbs the microwave energy, the absorption cannot be localized. A traveling ionization front is observed to proceed toward the radiation source. Fig. 3 shows the time history of the ionization front in the strong

mismatch case $I \gg I_B$ and $\tau_p > \tau_C$. The critical time τ_C is the time required for the electron avalanche to reach the critical density $n_C \equiv \omega^2 m_e / 4\pi e^2 \approx 10^{13} / \lambda^2$ (cm) where λ is the wavelength of the incident radiation. In this simulation $I = 12.5 \text{ kW/cm}^2 \gg I_B = 3 \text{ kW/cm}^2$, $\tau_p = 0.5 \text{ } \mu\text{sec}$, $\tau_C = 0.16 \text{ } \mu\text{sec}$, and all hydrodynamic effects are suppressed. The initial electron density (pre-ionized plasma) was initialized with a symmetric profile with a peak density of $0.1n_C$ and FWHM of 0.1λ . In Fig. 3, the peak density is determined by Eq. (10). However, the breakdown time, τ_B , is a complicated function of the incident and reflected microwaves. It is clear that the small reflectivity ($R < 10\%$) is important in determining the propagation speed since as Fig. 3 shows, the separation distance between peaks is $\lambda/4$. The ionization front proceeds toward the source at a characteristic speed $D(t) = \lambda/4\tau_C(t)$. The maximum density is decreasing with time while the total absorption continues to increase with time. The asymptotic absorption efficiency is approximately 95%. The movement of the ionization front limits the time the gas-plasma systems samples the radiation field. The sampling time, τ_S , is determined by $\alpha(\text{cm}) = \int_0^{\tau_S} D(t) dt \approx D(0)\tau_S$ where $D(0) = \lambda/4\tau_C(0) \approx 1.6 \times 10^6 \text{ cm/sec}$ is the early breakdown speed. Estimating the absorption length as $\alpha(\text{cm}) \approx \lambda/2\pi$ gives a sampling time of $\tau_S \approx \tau_C$. In the pressure regime $P > 25 \text{ Torr}$, the gas is primarily heated through the quenching of the electronic states by molecular and atomic nitrogen. The fractional change in the gas temperature is $\epsilon_g \equiv (\Delta T_g / T_g)_{\text{Max}} = \tau_S \Sigma_{\alpha\beta} Q_{\alpha\beta} n_\alpha n_\beta \epsilon_\alpha / c_v n_m T_g$ where $Q_{\alpha\beta}$ is the quenching rate of the N_2 triplet state n_α by the quenchant n_β . The specific heat of nitrogen is c_v and ϵ_α is the energy level of the n_α state. As an example, the $N_2(C^3\Pi)$ state is quenched by N_2 with a rate coefficient¹⁶ of $1.2 \times 10^{-11} \text{ cm}^3/\text{sec}$. The fractional change in the gas temperature, ϵ_g , is approximately 21% from the ambient temperature.

The region of the maximum gas heating is at the initial breakdown site ($\approx \lambda/4$ from the surface). The electric field is less than

1% of the incident time average electric field at the maximum gas temperature (Fig. 4a). The plasma absorbs approximately 70% of the incident microwave energy and has an electron temperature of less than 2.5 eV (Fig. 4b). Maximum gas heating requires the sampling time and the electron temperature to be as large as possible without decoupling the system. A high electron temperature populates the electronic states which are rapidly quenched to heat the gas. Approximately 4% and 40% of the incident energy goes into heating the gas and exciting the vibrational states. A similar simulation with the peak power reduced to $I = 6.25 \text{ kW/cm}^2$ shows no movement of the initial ionization region while increasing the fractional change in the gas temperature to 27%. Further irradiance would increase the gas temperature. However, these results are sensitive to the hydrodynamic response of the plasma. Again, a similar simulation with hydrodynamic effects showed a reduction in the gas and vibrational temperature. The microwave plasma system again decoupled; however, the hydrodynamic motion reduced the energy input into the gas and vibrational energy to 0.1% and 26% respectively. The electron density scale lengths are sharp, $L/\lambda > 10^{-2}$ where $L \equiv n_e(dn_e/dx)^{-1}$. The hydrodynamic motion of the electrons tends to reduce the electron temperature and density in regions of high density. The slow gas flow ($< 300 \text{ cm/sec}$) further reduces the electron temperature by convecting the vibrational energy away from regions of high electron density. The small temperature and density changes translate to greater than 10% reduction in the population of the electronic states. Since quenching of the electronic state is the dominant mechanism for rapidly heating the gas, the gas heating is negligibly small. It is clear that the motion of the ionization front will certainly limit the gas heating.

3.3 Gas Breakdown in a Focused Microwave System

Simulations of a focused microwave system were also performed. If the field intensity in a focused system greatly exceeds the breakdown threshold at the focal spot, a breakdown wave propagates toward the source.¹⁷ The motion of the microwave plasma absorbing layer is not a

simple breakdown wave, since the reflected microwave is important in determining the propagation speed. Fig. 5 shows the time history of the electron density profile during the course of a $\tau_p = 0.5 \mu\text{sec}$ pulse in a focused system. The spherical wave equation is solved for the electric field to model the convergence of the field. The peak incident field is $I = 10 \text{ kW/cm}^2$ with a system aspect ratio of 2.5. The average power at focus is 31.25 kW/cm^2 , and all hydrodynamic effects are suppressed. The very rapid early time speed of the absorbing wave, $D \approx 5 \times 10^6 \text{ cm/sec}$, gives a sampling time of $\tau_S \approx 1.7 \times 10^{-8} \text{ sec}$. However, the gas continues to be heated after the passage of the field by the de-excitation of the electronic states. The maximum gas and vibrational temperatures are $\epsilon_g \approx 10\%$ and $\epsilon_v \approx 260\%$ respectively. The quarter-wavelength fine structure in the density profile shows the effect of the reflected light. The time average reflection and absorption coefficient are 19% and 68% respectively. A snapshot of the electric field and electron temperature (Fig. 6) shows the lack of field penetration ($\alpha \approx 0.1\lambda$) and the cold plasma temperature, $T_e < 3.3 \text{ eV}$. The gas and vibrational temperatures again are reduced when hydrodynamic effects are included in the simulations. The gas is expected to be heated, at most, to 10% of the initial value during the course of a $0.5 \mu\text{sec}$ pulse.

The propagation velocity of the breakdown wave in a focused microwave system can be calculated. Simulations show the absorption is localized at the head of the breakdown wave. The reflection coefficient is relatively constant after the initial breakdown ($t > \tau_C$). The breakdown time, τ_B , is inversely proportional to the light flux, $1/\tau_B \propto (1 + 2\text{Re}\zeta + \zeta^2)I$, where the reflection coefficient is ζ^2 . The intensity in a conically focused system can be written as

$$I(\chi, t) \propto \frac{(1 + 2\text{Re}\zeta + \zeta^2)}{r^2} \times \phi(t)$$

where $\phi(t)$ is a form function characterizing the pulse. The radius of the radiation channel at a position X on the channel axis is $r = r_0 + X \tan \theta$. The minimum radius of the waist at the focal point is r_0 and θ is the half-angle of the radiation column. Following Raizer,¹⁷ the propagation velocity of the breakdown wave is approximately $D = r_0 / \tau_C \tan \theta$. Under the assumptions made, the velocity D would be an upper bound on the propagation velocity of the breakdown wave.

4.0 Simulation of the NRL Experiments

We compare the simulation results with the NRL experiment. The NRL 35 GHz 112 kW focused gyrotron system gives an average power at the focal spot of 33 kW/cm². The polarization of the microwave is such that the electric field is perpendicular to the plasma gradient (S polarization). The average aspect ratio of the experiment gives an equivalent simulation aspect ratio of 2.5. The free nitrogen breakdown experiments were performed at 25 Torr with a 100 pps repetition rate at $\tau_p = 1.5$ μ sec. The minimum radius of the waist at the focal spot is $r_0 = 0.75$ cm and the half-angle of the radiation column satisfies $\tan \theta = 0.35$. Experimentally, framing camera data (Fig. 7) gives a propagation velocity of $D = 4.6 \times 10^6$ cm/sec. The width of the absorbing wave is approximately 1.2 cm. The measured absolute intensity of the second positive band, N₂ 2P (0-0) at 3371 Å is 1.4×10^{21} eV/cm²-sec. The calculated spatial width of the 3371 Å light emission is 0.8 cm with a peak intensity of 1.8×10^{21} eV/cm²-sec. As mentioned previously, the calculated speed of the breakdown wave is 5×10^6 cm/sec. Experimentally, the inferred breakdown time is $\tau_B = 2.5 \times 10^{-8}$ sec or $\tau_C = 7.4 \times 10^{-7}$ sec. This is to be compared to the calculated breakdown time early in the pulse, $\tau_B = 4.5 \times 10^{-9}$ sec, and late in the pulse, $\tau_B = 6 \times 10^{-8}$ sec. The simulation results are felt to be in reasonable agreement with the experiment.

5.0 Conclusion

In conclusion, computer simulation of microwave coupling to a weakly ionized nitrogen gas plasma shows excellent absorption of the microwave energy. The electronic states of nitrogen excited by electron impact are rapidly quenched by molecular and atomic nitrogen to heat the gas at pressures above 25 Torr. However, high power irradiance can easily produce a non-hydrodynamic ionization front which can severely limit the heating of the gas. Microwave gas breakdown experiments with pulse lengths less than one microsecond are expected to show only a slight heating of the gas.

REFERENCES

1. A. D. MacDonald, Microwave Breakdown in Gases, John Wiley and Sons, Inc. (New York, 1966).
2. S. C. Lin and G. P. Theofilos, *Phys. Fluid* 6, 1369 (1963).
3. W. E. Scharfman, et al., *IEEE Trans. Antennas and Propagation* 12, 709 (1964).
4. W. M. Bollen, et al., "High Power Microwave Energy Coupling to Nitrogen During Breakdown," NRL Memo Report (in press).
5. C. L. Yee and A. W. Ali, "Microwave Energy Deposition, Breakdown and Heating of Nitrogen and Air," NRL Memo Report 4617 (1981).
6. J. O. Hirschfelder, C. F. Curtiss, and R. B. Bird, Molecular Theory of Gases and Liquids, John Wiley and Sons, Inc. (New York, 1964).
7. J. W. Rich, *J. Appl. Phys.* 42, 2719 (1971).
8. R. Millikan and D. White, *J. Chem. Phys.* 39, 3209 (1963).
9. Kinetic Processes in Gases and Plasma, edited by A. R. Hochstim (Academic, New York, 1969), Chaps. 2 and 3.
10. A. W. Ali, "The Physics and Chemistry of Two NRL Codes for the Disturbed E and F Regions," NRL Memo Report 7578 (1973).
11. G. J. Schulz, *Phys. Rev.* 135, A 988 (1964); H. Ehrhardt and R. Willman, *Zeits. Phys.* 204, 462 (1967); A. G. Engelhardt, et al., *Phys. Rev.* 135, A 1566 (1964).
12. R. B. Bird, Transport Phenomena, John Wiley and Sons, Inc. (New York, 1960).
13. E. L. Rubin and S. Z. Burstein, *J. Computational Phys.* 2, 178 (1967).
14. Y. B. Zel'Dovich and Y. P. Raizer, *Soviet Physics JETP* 20, 772 (1965).
15. Wee Woo and J. S. DeGroot, "Analysis and Computations of Microwave-Atmospheric Interaction," University of California, Davis, Department of Applied Science, Plasma Research Group Report 1981.
16. P. Millet, et al., *J. Chem. Phys.* 58, 5839 (1973).
17. Y. P. Raizer, *Soviet Physics JETP* 21, 1009 (1965).

FIGURE CAPTIONS

- Fig. 1 The breakdown time and the electron temperature vs. the rms electric field to density ratio E/n_m .
- Fig. 2 Gas breakdown near a reflecting surface showing the electron density pancakes for (a) one-and-a half, and (b) three wavelengths planar system. The critical density is $n_c = 1.5 \times 10^{13} \text{ cm}^{-3}$ and $k = 7.33 \text{ cm}^{-1}$.
- Fig. 3 Time history of the ionization front in a planar system showing the wave motion toward the radiation source. The microwaves are incident from the left onto a pre-ionized plasma near a reflecting surface on the right boundary. The normalization parameters are the same as in Fig. 2.
- Fig. 4 (a) The time averaged electric field square and (b) the electron temperature vs. position. The normalization parameters are: $T_{e0} = 0.25 \text{ eV}$, $k = 7.33 \text{ cm}^{-1}$, and the arbitrary units of $\langle E^2 \rangle = 1$ corresponds to an average intensity of 9.4 kW/cm^2 .
- Fig. 5 Time history of the ionization front in a spherical system. The microwaves are incident from the left boundary with an intensity of 5 kW/cm^2 . The focused average power is 31.25 kW/cm^2 at the right side boundary.
- Fig. 6 (a) The time averaged electric field square and (b) the electron temperature vs. position for the simulation of Fig. 5. The normalization parameters are the same as in Fig. 4.
- Fig. 7 Framing camera data showing the motion of the ionization front in a focused free nitrogen breakdown experiment. The top and bottom photographs were respectively taken 0.2- and 0.1- μsec after the first observable breakdown.

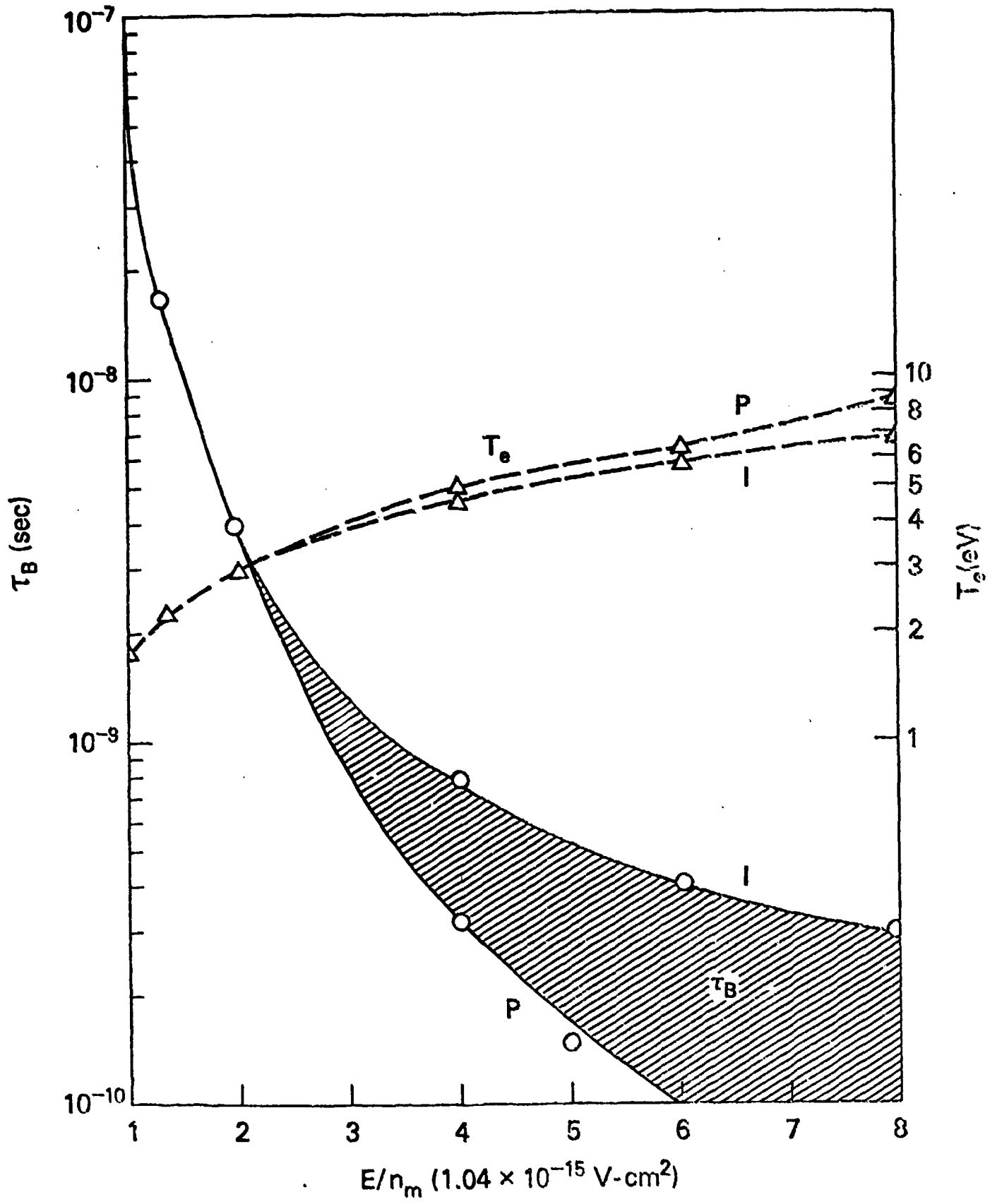


FIGURE 1

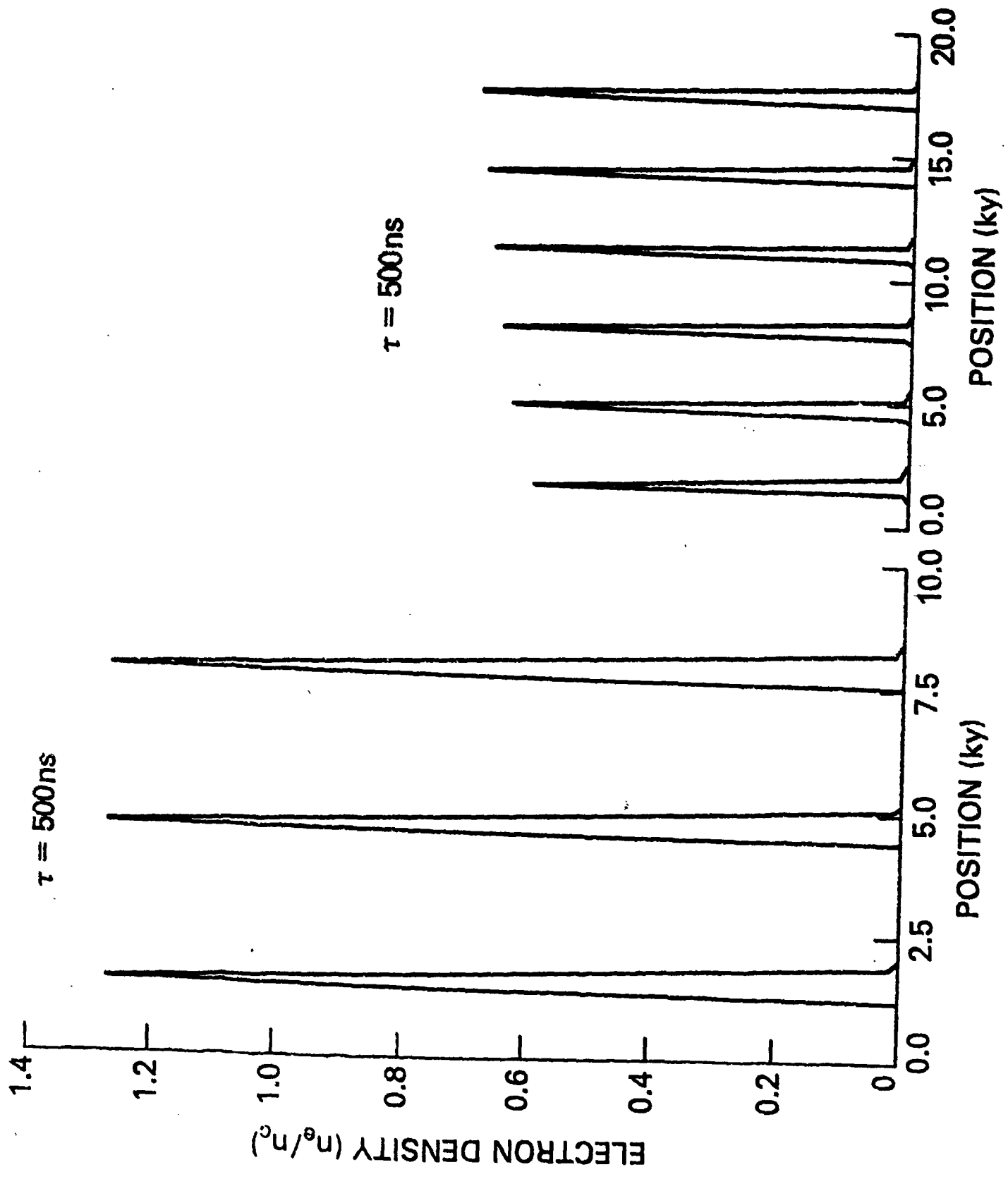


FIGURE 2

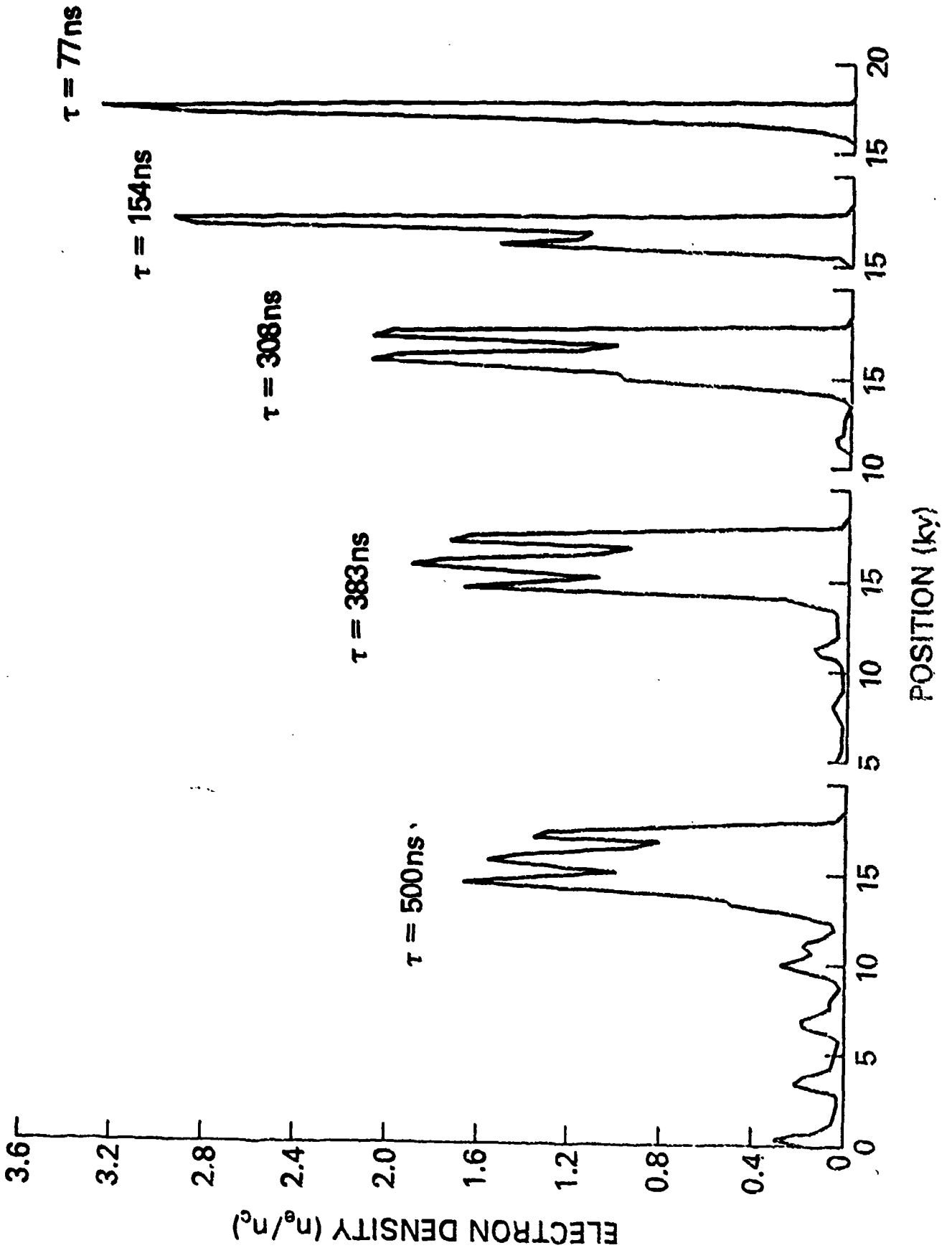


FIGURE 3

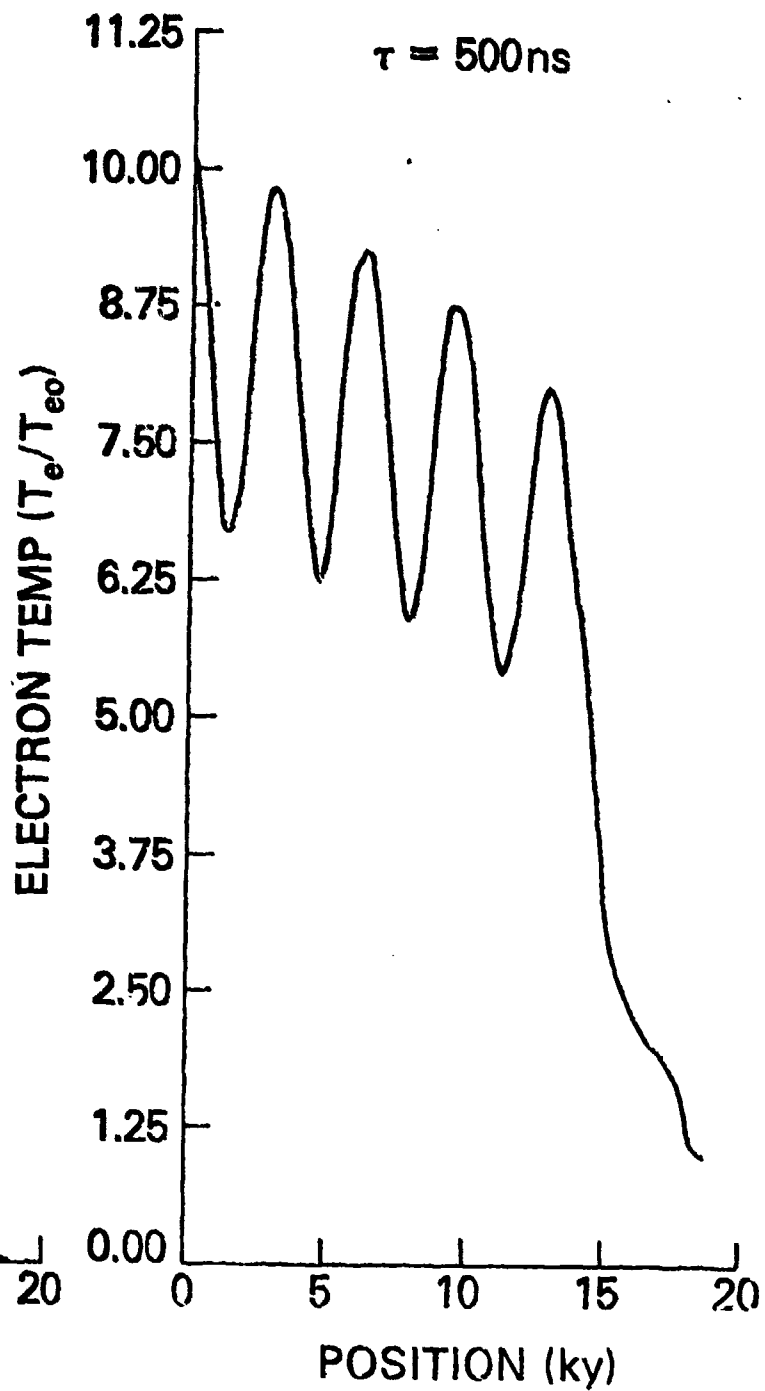
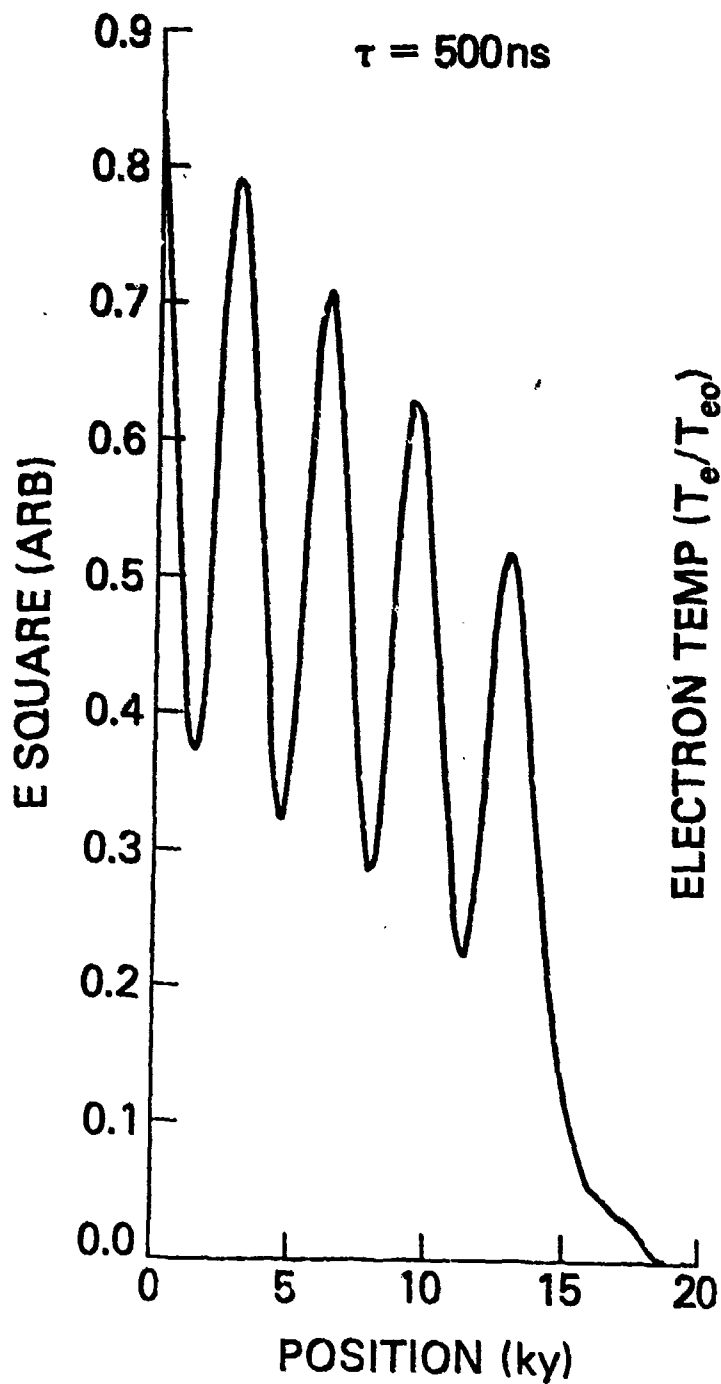


FIGURE 4

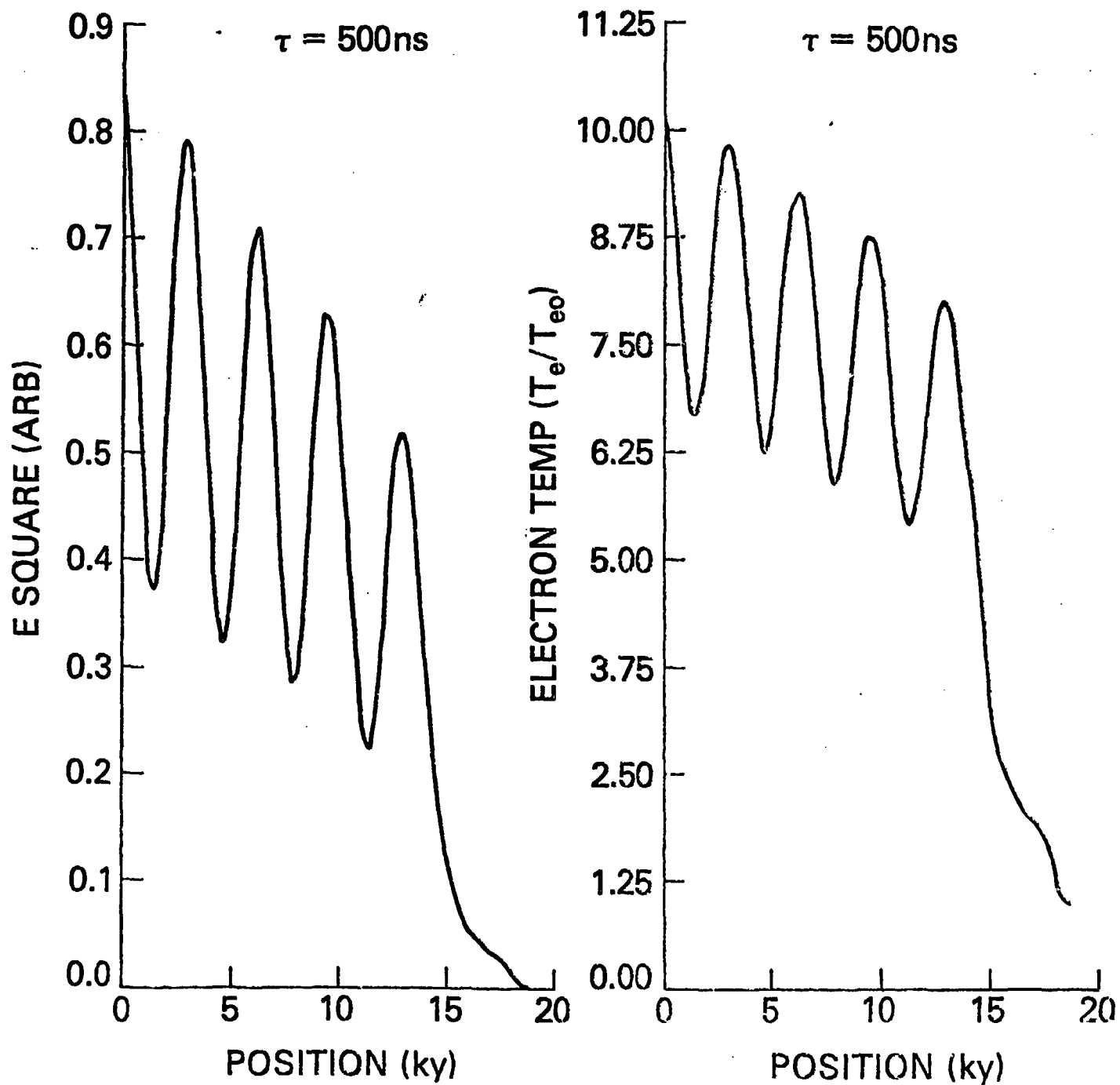


FIGURE 4

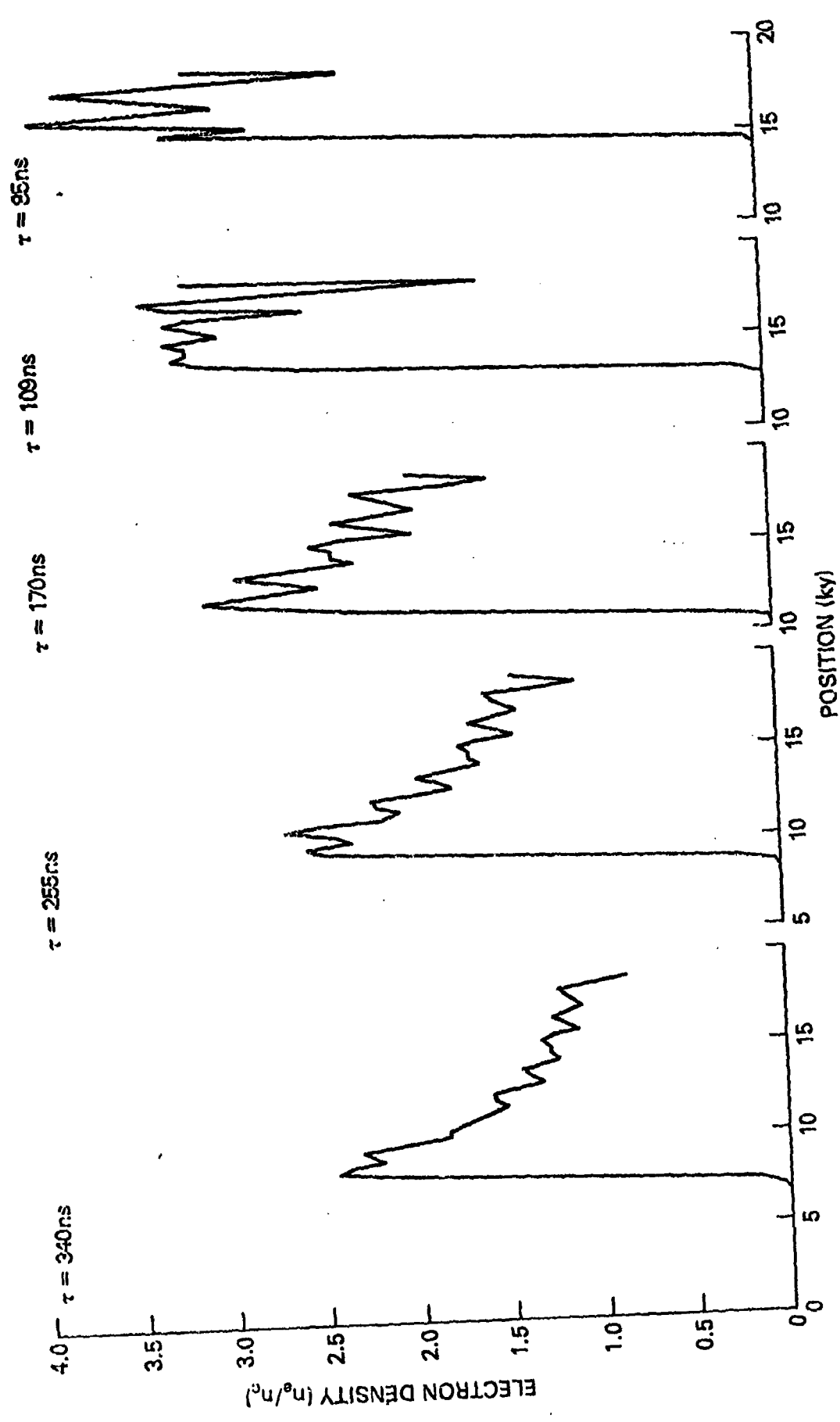


FIGURE 5

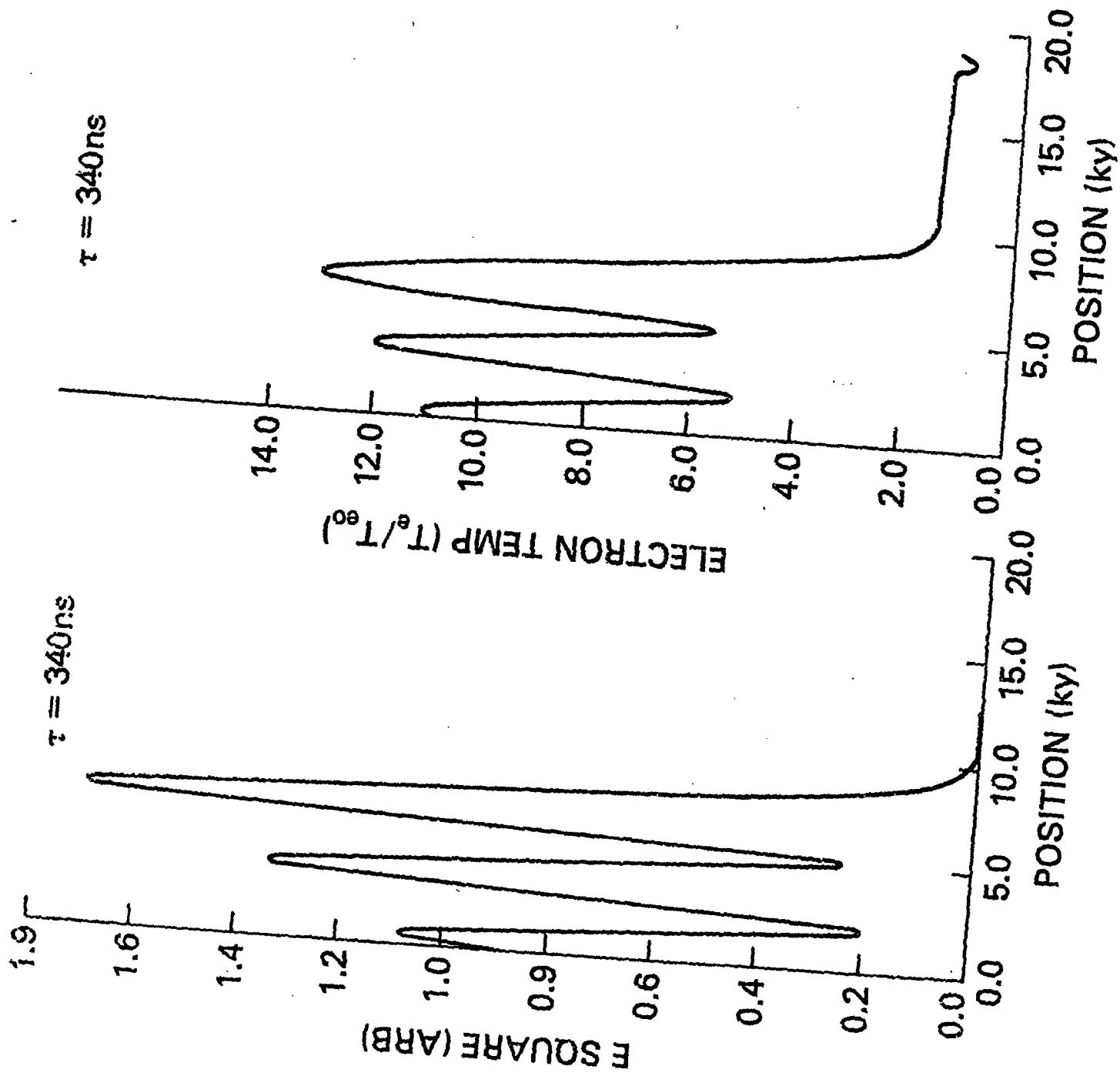
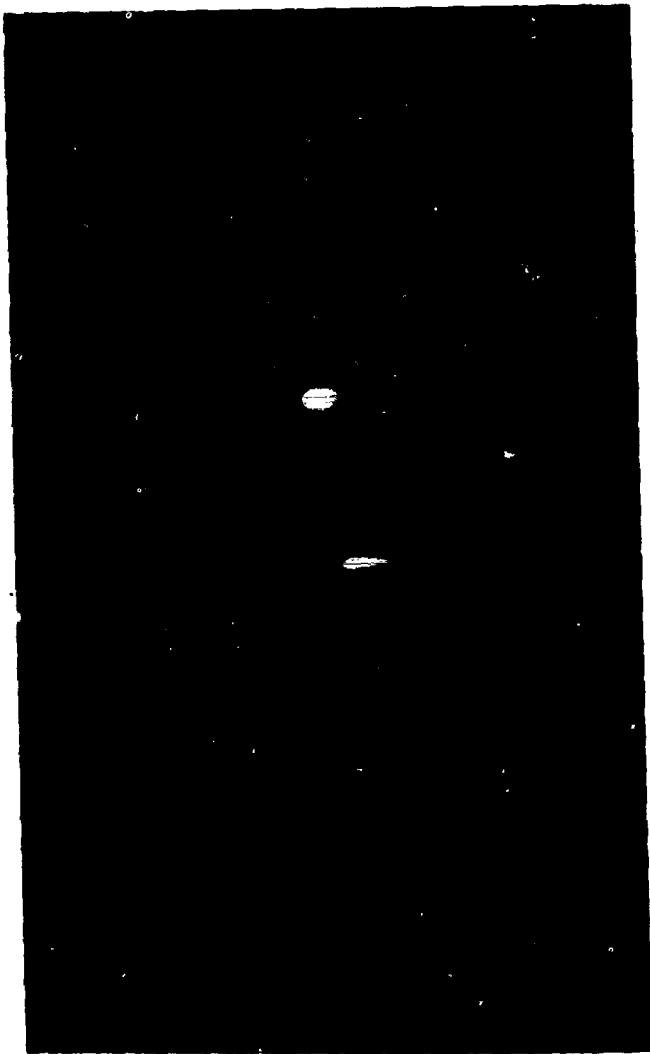


FIGURE 6



10 cm

FIGURE 7

APPENDIX C

High Power Microwave Energy Coupling to Nitrogen During Breakdown
W. M. Bollen, C. L. Yee, A. W. Ali†, M. J. Nagurney,
and M. E. Read†

ABSTRACT

Microwave energy coupling to nitrogen for breakdown conditions have been investigated. The experiments were performed in 25 Torr nitrogen using a 35 GHz 1 μ s microwave pulse focused to 33 kW/cm². The plasma created during breakdown was observed to travel towards the source with a velocity of 4.6×10^6 cm/s. Spectroscopic measurements using a nitrogen helium mixture indicate the average electron density over a 2 cm cord to be 4.4×10^{12} cm⁻³, and the electron temperature to be 3.8 eV. Microwave cutoff was observed photographically and suggests the peak electron density to be the collisional critical density. Computer simulations were also performed and their results are in accord with the experimental results.

† Naval Research Laboratory

I. INTRODUCTION

Microwave breakdown studies of gaseous elements have been carried out extensively over a wide range of pressures and for several microwave frequencies using CW and pulsed radiation sources¹. The main emphasis on these studies was the determination of the breakdown power threshold, and its dependence on the gas pressure and the microwave frequency. The coupling of microwave energy into the breakdown plasma and neutral gas has not been studied in detail. The reason for this is that until recently no high power microwave sources have been available to perform such studies. Most of the early work performed on breakdown thresholds was performed using high Q cavities to obtain the necessary electric field to break down the gas. Once breakdown of the gas occurred, the Q of the cavity dropped and the interaction changed. Using the NRL high power gyrotron facility, we have been able to eliminate the need for cavities and have performed experiments using a focused geometry² to examine the coupling of microwave energy to nitrogen gas during breakdown. We have also modeled the experiments using a 1-D computer simulation code³. Simulations were performed in a spherical geometry using a self-consistent, nitrogen chemistry, wave optics, microwave breakdown simulation code, MINI.

The main emphasis of this paper is on the ionization front created during nitrogen breakdown and its motion and plasma properties as observed experimentally. This motion is not a movement of the plasma but rather a movement of where the strongest ionization of the gas is taking place. We believe it to be due to two effects: 1) delayed ionization and 2) reflection from the plasma itself. Since the electron density is proportional to e^{tI_0} , where I_0 is the local microwave intensity, breakdown occurs faster in those regions of high intensity. In a focused system this results in breakdown beginning at the focus. The breakdown

then moves back into the lower intensity region as time progresses. If nothing else is occurring, one would then observe a cone of plasma late in time. However, the plasma is both absorptive and reflective. The reflection results in standing wave patterns. Thus peaks $\lambda/2$ apart are seen to grow in time. The first peak is $\lambda/4$ from the plasma surface. As the density increases in these peaks, they become reflective and absorptive, cutting off the microwave energy to peaks behind them. Again, the density grows as $e^{at}I_0$, and, therefore, those peaks nearest the focus initially grow fastest. If only one peak were reflecting, we would expect $\lambda/2$ structure. However, all the peaks reflect and, therefore, we expect $\lambda/4$, the distance from the reflecting surface to the first electric field maximum, to occur as well. Thus, in the experiment, we would expect a background plasma due to delayed ionization with $\lambda/2$, and $\lambda/4$ structures in it due to reflection. Reflection and absorption will also prevent microwave penetration, so we expect to see the plasma disappear behind the front of the ionization. This results in the appearance of motion. This motion may then occur as $\lambda/2$ or $\lambda/4$ jumps, since once these structures develop, the intensity at these points is larger, due to reflection, than the background intensity.

This ionization front motion strongly affects the coupling of microwave energy to the gas. It determines where the energy will be absorbed, since its high density does not allow microwave penetration. Also, since it is moving, it spreads the heating out in the gas. Motion towards the microwave source has been observed by Salisbury and Flint⁴, and by Beust and Ford⁵. The velocities were much slower, however, $V \approx 3 \times 10^3$ cm/s for Salisbury and Flint's work, and $V \approx 600$ cm/s for Beust and Ford's work. Raizer⁶ advanced a theoretical treatment for the microwave discharge propagation in high pressure air (~ 1 Atm) to explain Beust and Ford's results under CW conditions. Other work by Scharfman, et al⁷, observed that for low pressures the breakdown plasma became opaque to microwaves, thus preventing penetration. We have observed the formation of the front, its motion, the prevention of microwave penetration, and

measured the plasma density and electron temperature of the front. Good agreement was found between the experiment and the simulation model.

II. EXPERIMENT

A. Apparatus

The microwave energy coupling experiments were performed in dry nitrogen using one of the NRL 35 GHz, high power gyrotrons⁸. This gyrotron is capable of 150 kW, 1 μ sec pulses at 100 pps. The investigation, however, was performed with a microwave power \approx 112 kW using S polarization. The nitrogen pressure was variable. The data presented is at a pressure of 25 Torr which corresponds to $\nu/\omega \approx 0.65$, where ν is the collision frequency for electron momentum transfer and ω is the natural frequency of the microwave radiation. The microwave radiation is introduced into a test chamber using a conical horn with a focusing dielectric lens in front, see Figure 1. The lens has a focal length of 11.2 cm and a diameter of 7.62 cm. The focal spot is elliptical and has an approximate gaussian distribution in intensity with half widths of 1.5 cm and 1.1 cm. The 3dB focal spot area is approximately 1.7 cm². For 112 kW this implies 33 kW/cm² average power inside the 3dB spot. Breakdown, without a reflecting surface, was observed to cease at $p \approx 75$ Torr for $P = 112$ kW. Theoretically, we calculate an average power of 27 kW/cm² is required for breakdown at 75 Torr in nitrogen. This is in reasonable agreement with an estimated intensity of 33 kW/cm². We have, however, ignored the gaussian spread and assumed an even distribution.

The breakdown experiments were performed with and without a metal surface at the focal point. The planar metal surface could be oriented perpendicular, 90°, or with an angle of 45° to the incident radiation. The metal surface serves to set up a standing wave pattern in

front of the surface resulting in $4 I_0$ at the peaks, where I_0 is the intensity of the incident radiation. Also, a thin dielectric could be placed off the metallic surface. This was used in determining the cause of the plasma motion observed and will be discussed later.

Observation of the plasma was done using a TRW framing/streaking camera. A 20 ns exposure time was used in the framing mode and a 2 μ s exposure time in the streaking mode. Due to the amount of light present, multiple exposures were required in order to obtain easily visible photographs. However, some single shot experiments were performed and showed that the results were reproducible shot-to-shot. The electron temperature and density were measured by using a nitrogen-helium gas mixture. In a pure nitrogen mixture, only second positive nitrogen bands were observable. By introducing helium, the 5876A line could be used with the nitrogen 3371A band to make the required density and temperature measurements. An Oriel model 7240 monochromator, f/3.7, with a 10A bandwidth was used. The monochromator output was measured using a 1P28 photomultiplier with a base modified for nanosecond response time. Absolute intensity calibrations were performed using a calibrated deuterium arc lamp source⁹ for 3371A and a calibrated strip tungsten lamp source¹⁰ for 5876A.

Our experiments were performed at 25 Torr where we had approximately nine times the intensity required to break down the nitrogen at the focal spot. With the presence of a metal surface, a factor of four reduction in the power required for breakdown occurs due to the standing wave pattern which is set up. Due to the focused nature of the experiment, the standing wave pattern's intensity drops as the distance from the surface is increased. For the 45° target, in fact, there is only a small region of standing waves perpendicular to the surface. It is only for the 90° surface, or the case of a reflective plasma perpendicular to the microwave beam, that a standing wave pattern back the length of the beam line exists. A delayed breakdown from the surface back towards the lens

is then expected, since the growth of the plasma is proportional to e^{tI_0} . We believe that fluctuations in the reflective plasma surface and UV ionization (if any) will cause a smearing out of the standing wave pattern.

B. Discussion of the Experimental Results

1. Time Resolved Photographs of Breakdown

The observed breakdown patterns for the three cases are shown in Figures 2 through 4. In Figure 2, the breakdown without a surface is shown. A conical plasma is formed with its tail nearest the focal point and head towards the lens. This indicates that a large fraction of the microwave energy is concentrated on axis. For a diffraction limited spot size we calculate the depth of field (where $I = I_0/e$) for our case to be 3.5 cm which is approximately the length of the tail in the early breakdown region observed in Figure 2. The total length of the breakdown region is 5 cm. We calculate a length of 3.7 cm based on incident intensity decreasing to the nitrogen breakdown threshold as we move away from focus. This suggests reflection off the plasma must be occurring. We calculate that $\approx 19\%$ reflection would be required; the simulation suggests $R \leq 28\%$. The breakdown begins at the focal spot, but since the microwave power is above the breakdown threshold, a secondary breakdown region ahead of the focus forms in a time $\approx 2.4 \times 10^{-7}$ s after the initial breakdown. As the electron density in this secondary breakdown region increases to $N_c = (\omega^2 + \nu^2)m_e/(4\pi e^2)$, the tail (focus) region disappears due to the microwaves being absorbed and reflected by the plasma at the head. Once the microwave energy is stopped from reaching the plasma in the tail, the plasma temperature there drops rapidly ($\tau \approx 10$ ns), and the emitted light ceases. The plasma itself also begins to decay, but on a longer time scale. Late in time we see that a single absorbing layer about one wavelength thick is formed.

Figure 3a shows the framing camera data for the perpendicular surface experiment and Figure 3b shows a streak photograph for the same case. We expect a standing wave to be set up off the surface with the first maximum $\lambda/4$ from the surface and with the rest of the maxima spaced $\lambda/2$ apart. This can be seen in Figure 3a. Also observed is a "blooming" of the visible plasma near the target. We believe this is an effect due to the focusing. The microwave beam becomes more intense near focus. Therefore, the diameter of the beam capable of breaking down the plasma increases. Similar to the no target case, an absorbing front travels away from the target towards the microwave source. From the displacement in the streak photograph, we calculate that the plasma moves away from the surface with a velocity = 4.6×10^6 cm/s. It continues to move back along the microwave beam until the beam energy decreases sufficiently (due to defocusing) that the beating with any reflected microwaves is below the breakdown threshold. This "stagnation point" is also observed for the 45° surface. Similar behavior is also observed in the computer simulation.

The 45° data is shown in Figure 4. It is similar to the 90° data except fringes occur $\lambda/(2 \cos \theta)$ apart, $\theta = 45^\circ$, with the first fringe at $\lambda/(4 \cos \theta)$ from the surface. Again, an absorbing front moving along the beam axis is observed. This occurs as a result of energy reflected by the plasma along the beam. Since we are far above threshold, we believe a planar plasma, perpendicular to the beam, grows near the target and is initiated by the plasma growth at the standing wave maxima. Its density grows ($N_e \rightarrow N_c$) and it becomes reflective, setting up standing waves. Plasma density builds at these maxima cutting off microwave penetration, and the process repeats. Visually, this appears as plasma motion. We would expect the motion to jump in either $\lambda/2$ or $\lambda/4$ steps. Some of the 45° data shows $\lambda/2$ bars behind the main moving plasma. In general, however, this is not observed. The $\lambda/2$ spacing is at about the limit of resolution. Further, we believe that fluctuations in the reflective plasma surface cause a smearing out of the standing wave

pattern and results in the more solid like appearance we observe for the moving plasma.

One other possible explanation for the front motion is that UV emission causes ionization to occur in front of the plasma. This new plasma absorbs microwaves, heats up, and then the process repeats. This would result in a uniform smear with no $\lambda/2$ structure. Our data is somewhat suggestive of this. To check this idea we placed a thin dielectric a few wavelengths off the metallic surface to stop UV penetration but allow microwave transmission. If UV ionization was the method of propagation, we expected the plasma to stop moving when it hit the dielectric. The plasma moved through the dielectric barrier. We, therefore, believe the motion to be due to reflection from the plasma itself resulting in ionization fronts. However, ionization due to UV may be responsible for some of the smearing of the $\lambda/2$ and $\lambda/4$ structure. The UV ionization mean free path is ≈ 0.05 cm $\ll \lambda/2$ for our conditions.

For the 45° target case the breakdown was examined as the power was decreased. As the power was decreased, the ionization front was observed to stagnate closer and closer to the target, as expected. When the incoming power was 20 kW, ≈ 5.9 kW/cm², we observed only two fringes and no apparent ionization front. At 30 kW the front reappeared. Incident radiation on a metal surface for breakdown to occur at 25 Torr is ≈ 0.75 kW/cm². However, we are only twice the free nitrogen breakdown threshold of 3 kW/cm², and this will be the dominant threshold for ionization front travel due to delayed ionization.

2. Spectroscopic Measurement of Density and Temperature

In order to measure the temperature and density of the electrons, the absolute intensity of the nitrogen second positive band, 3371Å, was compared to the absolute intensity of the neutral helium line at 5876Å. A mixture of the helium and nitrogen was used to perform this

experiment. The 3371Å band corresponds to the (0,0) transition in the second positive band system of N₂. We obtained the electron temperature from the ratio of the two lines¹¹ and the electron density from the absolute intensity measurement and the deduced electron temperature.

For an optically thin line and assuming a steady state coronal model, the band intensity at 3371Å can be expressed as:

$$I_{ul} = \frac{N_e N_2 X_{oc} A_{0,0} E_{0,0} L}{A_0 + q N_2} \quad (1)$$

where N₂ is the density of the nitrogen molecules in the ground state, X_{oc} is the emission excitation rate coefficient, A_{0,0} is the transition rate for the band at 3371Å and A₀ is the total transition rate for the excited state, E_{0,0} is the photon energy, L is the length of the emitting plasma, and q is the quenching rate coefficient of the excited state by the neutral species. A similar equation can be written for the intensity of the helium line. The excitation rate coefficients for 3371Å and 5876Å were obtained using the measured cross sections^{12,13} averaged over a Maxwellian electron velocity distribution. The transition rates for 3371Å and for 5876Å are from Refs. (14) and (15) respectively. The quenching rate coefficient¹⁶ for 3371Å by N₂ is 1.15 x 10⁻¹¹ cm³/sec.

The measured absolute intensities of 3371Å and 5876Å in a mixture of 15 Torr N₂ and 19 Torr He were 28.36 W/cm²sr and 5.6 x 10⁻² W/cm²sr. Using the above analysis, we obtain T_e = 3.8 eV and N_e = 4.4 x 10¹² cm⁻³ for the average density over a 2 cm chord. If quenching of the helium line by nitrogen is included the electron temperature changes slightly, T_e = 4.1 eV, with a corresponding slight decrease in the calculated electron density. This electron density is in reasonable agreement with Langmuir probe data, N_e ~ 2 x 10¹³ cm⁻³ and simulation predictions, N_e = 3.6 x 10¹³ cm⁻³ since these last two are peak local densities. It is reasonable to expect that the peak density is at least four times larger than the average density since the density is

proportional to $e^{I_0 t}$ and the microwave intensity is gaussian across the chord. (The two centimeter cord is slightly larger than the FWHM of the intensity gaussian.) A comparison of the absolute intensity of the 3371A nitrogen band for pure N_2 as observed experimentally ($I_{exp} = 1.12 \times 10^{20}$ eV/(cm²-s-sr)) agreed reasonably well with the simulation predictions for similar conditions ($I_{sim} = 3.6 \times 10^{20}$ eV/(s-cm²-sr)). As expected, the simulation also predicted a lower electron temperature, $T_e = 3.25$ eV, for the pure N_2 case.

III. COMPUTER SIMULATION

The breakdown experiments were modeled neglecting hydrodynamic motion and solving the electric field in spherical geometry¹⁷. Nitrogen breakdown experiments with no surface, Figure 2, show the microwaves penetrating approximately six wavelengths into the tenuous plasma early in time. The experimental light emission shows the electric field is essentially close to planar for regions near the focal point. However, for distances greater than 4 cm from the focal point, the electric field shows an abrupt transition to a spherical (converging) geometry. The ratio of the inner and outer radius in a spherical system defines an aspect ratio. The converging geometry of the experiment defines an aspect ratio of 3.2 in the converging region and 1.9 in the diffraction limited focal region (approximately planar). We modeled this using an aspect ratio of 2.5 in the simulation. (The simulation has shown that for larger aspect ratios the behavior is similar, but the front does not travel as far.) The simulation used a 0.5μs pulse length, τ_p , at an angular frequency, ω , of 2.2×10^{11} sec⁻¹ and an average power of 31.25 kW/cm² at the focal point. The region modeled was three wave lengths long (2.57 cm), had no reflecting surface, and a nitrogen pressure of 25 Torr. This simulation showed ionization front motion similar to that seen experimentally in Figure 2. This is shown in Figure 5 as a time history of the plasma density profile. The electric field drops rapidly beyond the peak electron density $N_e^{max} = 3.6 \times 10^{13}$ cm⁻³ and penetrates about

one and a half wavelengths into the overdense plasma (Figure 6a). The peak electron and gas temperatures are $T_e \approx 3.5$ eV (Figure 6b) and $T_g \leq 0.027$ eV, respectively. Breakdown simulations with hydrodynamic effects show similar features.

This same simulation was repeated with a reflecting surface at the focal point. Figure 7 shows the simulation results for the electron density. Close to the reflecting surface, the radiation is essentially planar and exhibits the characteristic standing wave pattern. Electron density "pancakes" form at the interference maximum of the electric field. However, at high power the electron density of the pancakes rises to $N_e \geq N_c$ at which time the radiation is partially reflected from the density pancakes. This shifts the breakdown patterns in increments of a quarter-wavelength. The quarter-wavelength fine structure of Figure 8 cannot be resolved experimentally. Similar to the free-nitrogen breakdown, approximately 79% of the incident microwave energy is absorbed. Early in time, the reflecting surface acts to enhance the field. However, once the density rises to absorb the radiation, the field reflects from the density pancakes. Though the reflection was small ($R < 28\%$), the effects of the reflection can also be seen for the no surface simulation in the quarter-wavelength fine structure of Figure 5.

The ionization front is observed to stagnate at about the same position in the experiment with and without a surface. This would only be true if the target is essentially decoupled from the microwave radiation and the absorption efficiencies are approximately equal. The simulations show this to be true with absorption efficiencies of 79% and 72% for breakdown with and without a surface. The simulations predict a front motion of $V \approx 5 \times 10^6$ cm/s early in the pulse and slowing to 2×10^6 cm/s when the simulation ends in $0.5 \mu\text{s}$. This gradual slowing of the ionization front is consistent with what is seen experimentally in Figure 3b.

IV. CONCLUSION

In conclusion, we have observed that for $I > I_B$, ionization fronts form and move towards the source at a velocity $\approx 4.6 \times 10^6$ cm/s. These ionization fronts result from both delayed ionization and reflection of microwave energy from the front. The front density can become quite large and is seen to cut-off microwave penetration in about one wavelength in late time. The average chord plasma density was spectroscopically measured to be $N_e = 4.4 \times 10^{12}$ cm⁻³ and the electron temperature to be $T_e = 3.8$ eV for a nitrogen-helium mixture. Langmuir probe measurements of the density gave reasonable agreement with peak densities for pure nitrogen of $N_e \approx 2 \times 10^{13}$ cm⁻³. The cut-off of microwave penetration observed photographically suggests an electron density $N_e = N_C = 2.2 \times 10^{13}$ cm⁻³. We expect the electron temperature in the gas mixture to be higher since N₂ vibrational and low lying electronic states act to decrease T_e and monoatomic He has no such states. Reasonable agreement was seen with the simulation for the velocity of the ionization front, N_e , T_e , and I_{3371} . The simulation predicts small reflection, $R < 28\%$, and low gas temperature, $T_g \leq 0.027$ eV.

FIGURE CAPTIONS

- Fig. 1 Schematic of nitrogen breakdown experiment. Shown as an insert is the 3dB focal spot.
- Fig. 2 Framing photographs of breakdown at 25 Torr N_2 for no surface present, $I_0 = 112$ kW or 33 kW/cm² at focus. The microwaves are incident from the left. Frames are 100 ns apart and have a 20 ns exposure time. Time shown on right refers to the delay after the first observable breakdown and not the microwave pulse.
- Fig. 3a Framing photographs at 25 Torr N_2 for 90° metal surface present at focus, $I_0 = 112$ kW. Times shown on right refer to the delay after first observable breakdown.
- Fig. 3b Streaking photograph at 25 Torr N_2 for 90° metal surface present at focus, $I_0 = 112$ kW. Streaking time was 2 μ s. The velocity of motion for the ionization front is measured to be 4.6×10^6 cm/s from the photograph.
- Fig. 4 Framing photographs at 25 Torr N_2 for 45° metal surface, $I_0 = 112$ kW. Times shown on right refer to the delay after the first observable breakdown.
- Fig. 5 Time history of the ionization front in a spherical system. The microwaves are incident from the left with an intensity of 5 kW/cm². The focused average power is 31.25 kW/cm² at the right hand boundary. An aspect ratio of 2.5 was used to model the experiment and N_c is the collisionless critical density.
- Fig. 6a Time average intensity for parameters of Figure 5. Units are in $\alpha = (V_{os}/V_{eo})^2$ such that $\alpha = 1$ corresponds to $I = 9.4$ kW/cm².
- Fig. 6b Electron temperature for parameters of Fig. 5 where $T_{eo} = 0.25$ eV.
- Fig. 7 Electron density profile at $t = 0.26\mu$ s into the pulse. Same parameters as in Fig. 5 except with a reflecting surface.

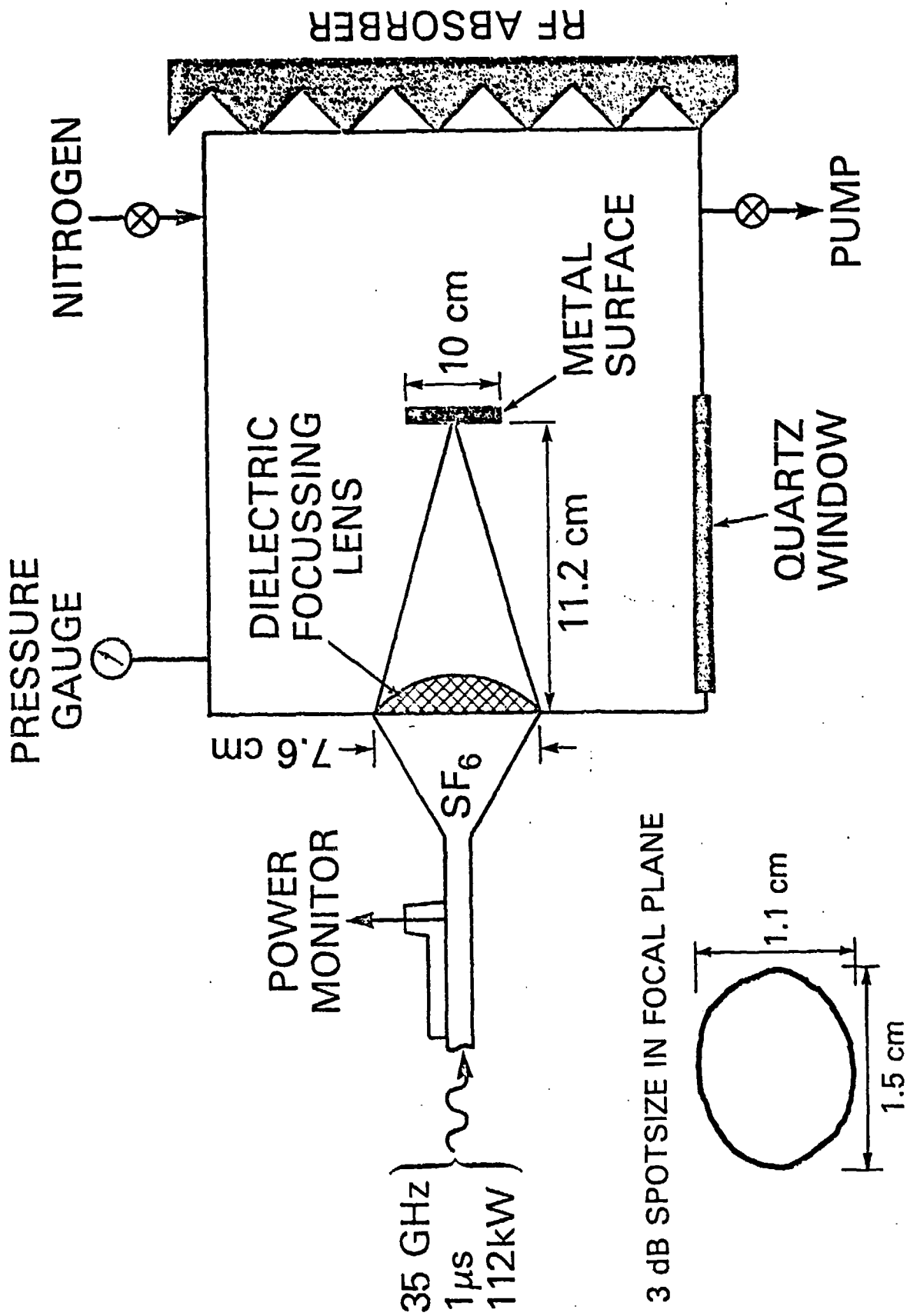


FIGURE 1

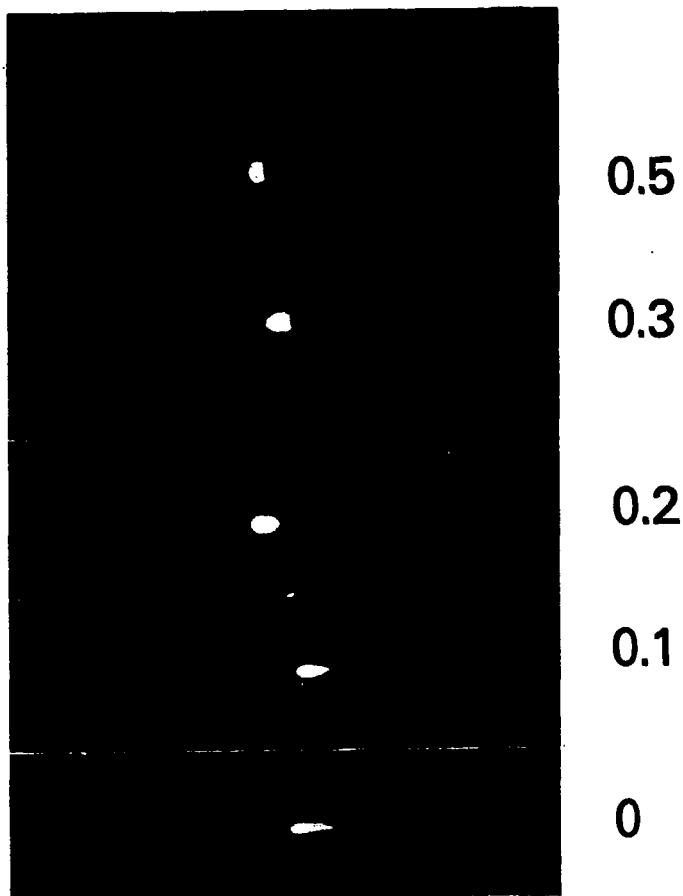
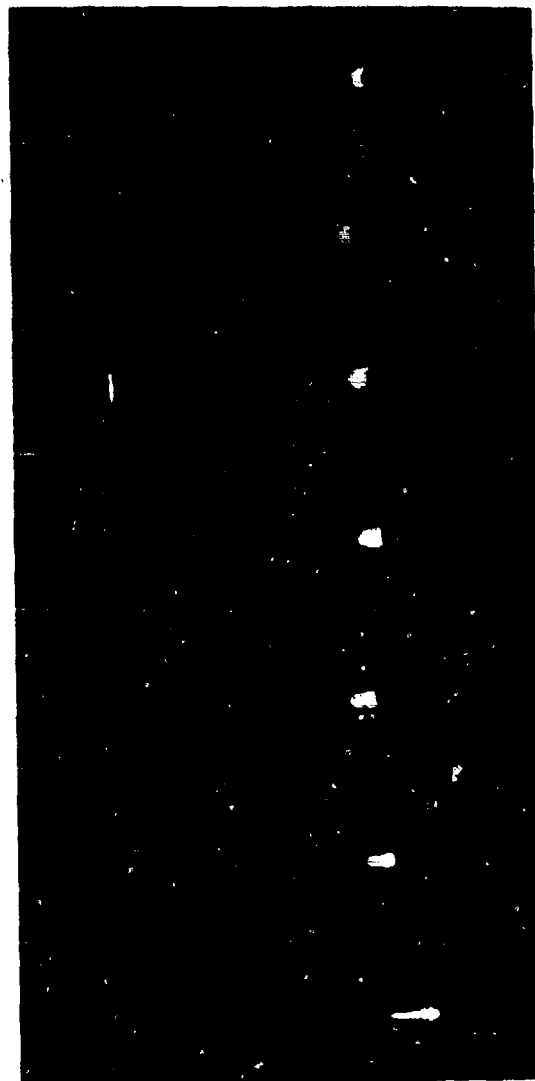


FIGURE 2



0.9

0.75

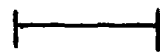
0.55

0.35

0.2

0.1

0.0



10 cm

FIGURE 3 (a)

C-15



2 μ s

10 cm

FIGURE 3(b)



1.0

0.7

0.5

0.35

0.25

0.1

0



10 cm

FIGURE 4

C-17

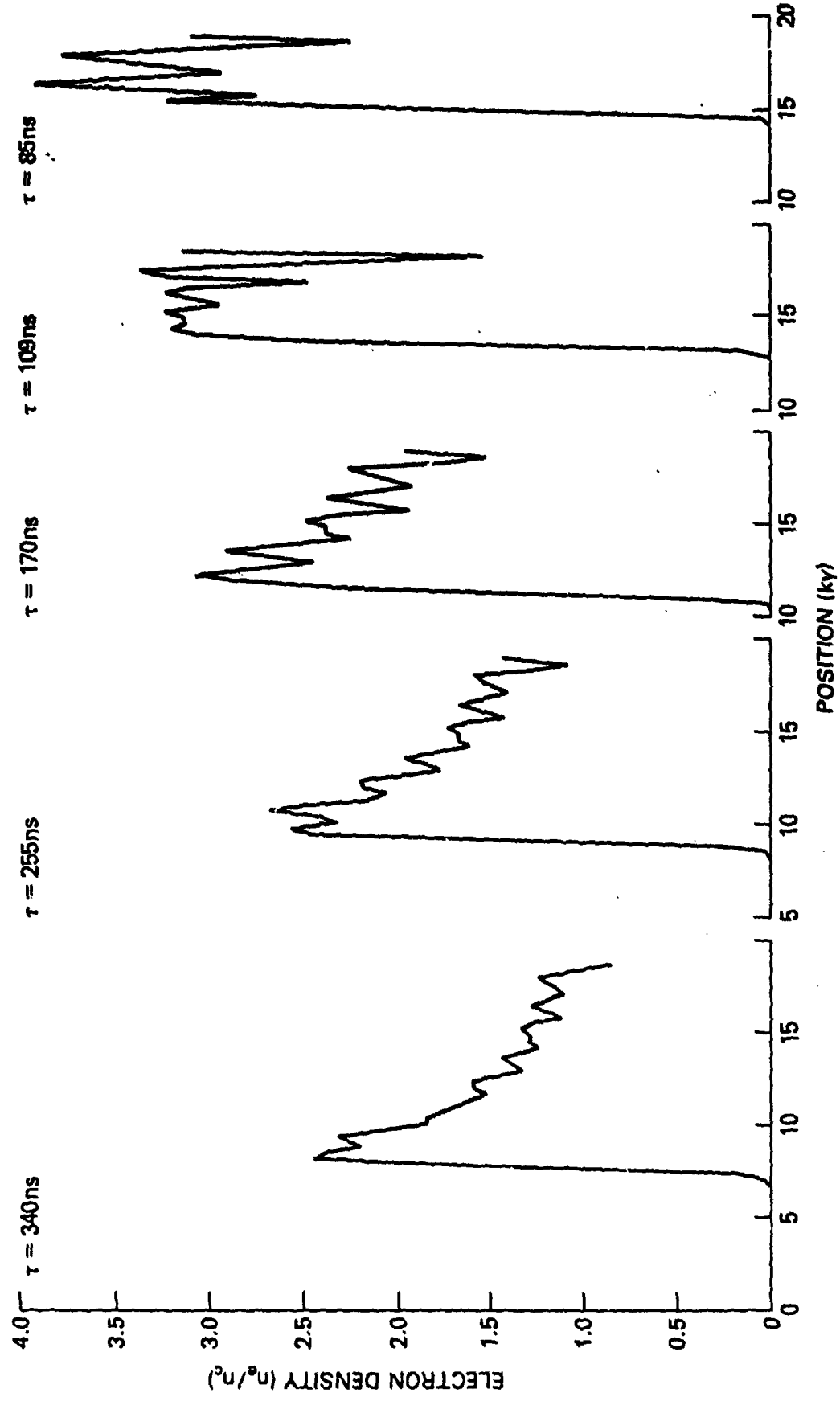
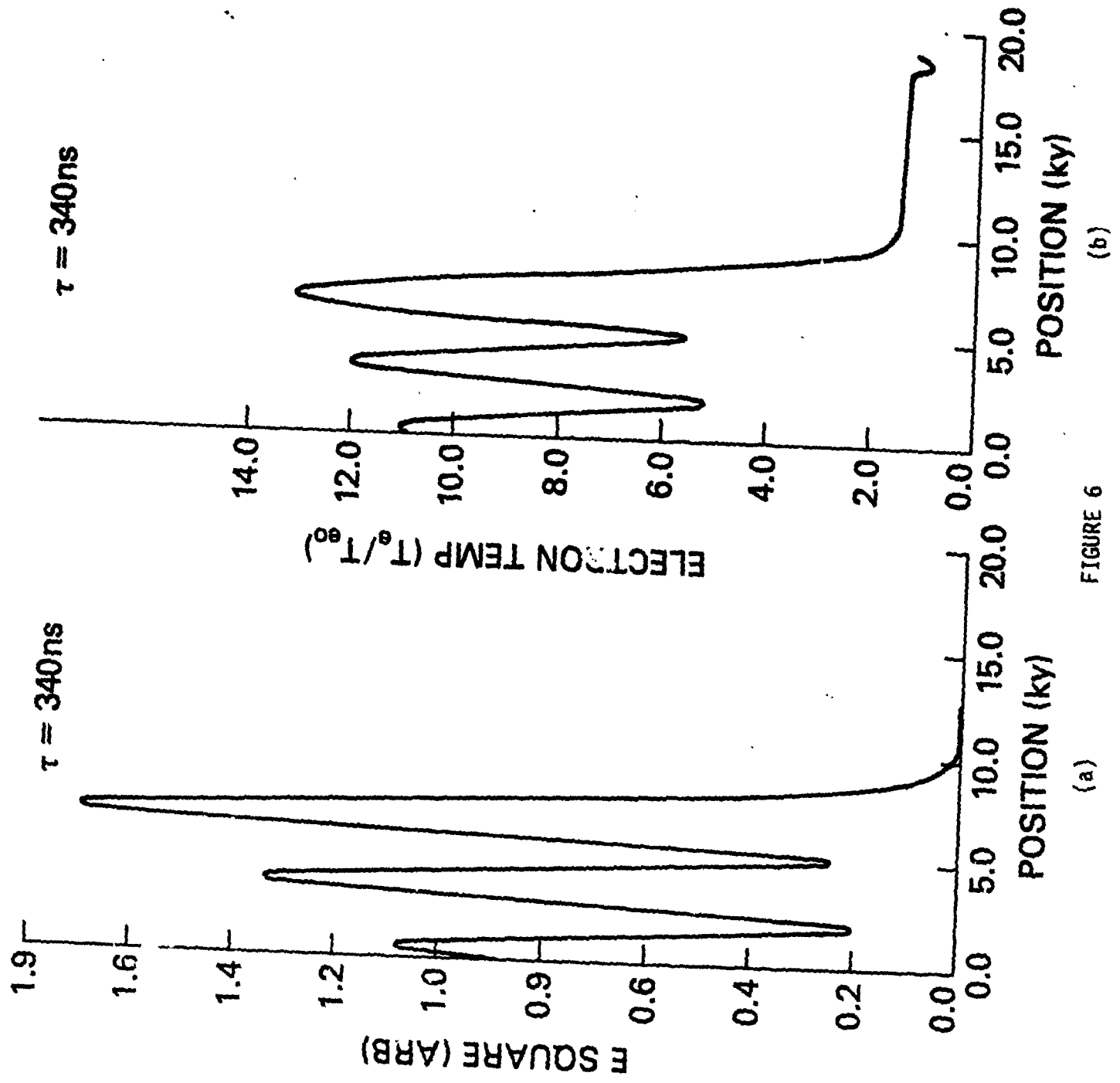


FIGURE 5



(a) FIGURE 6 (b)

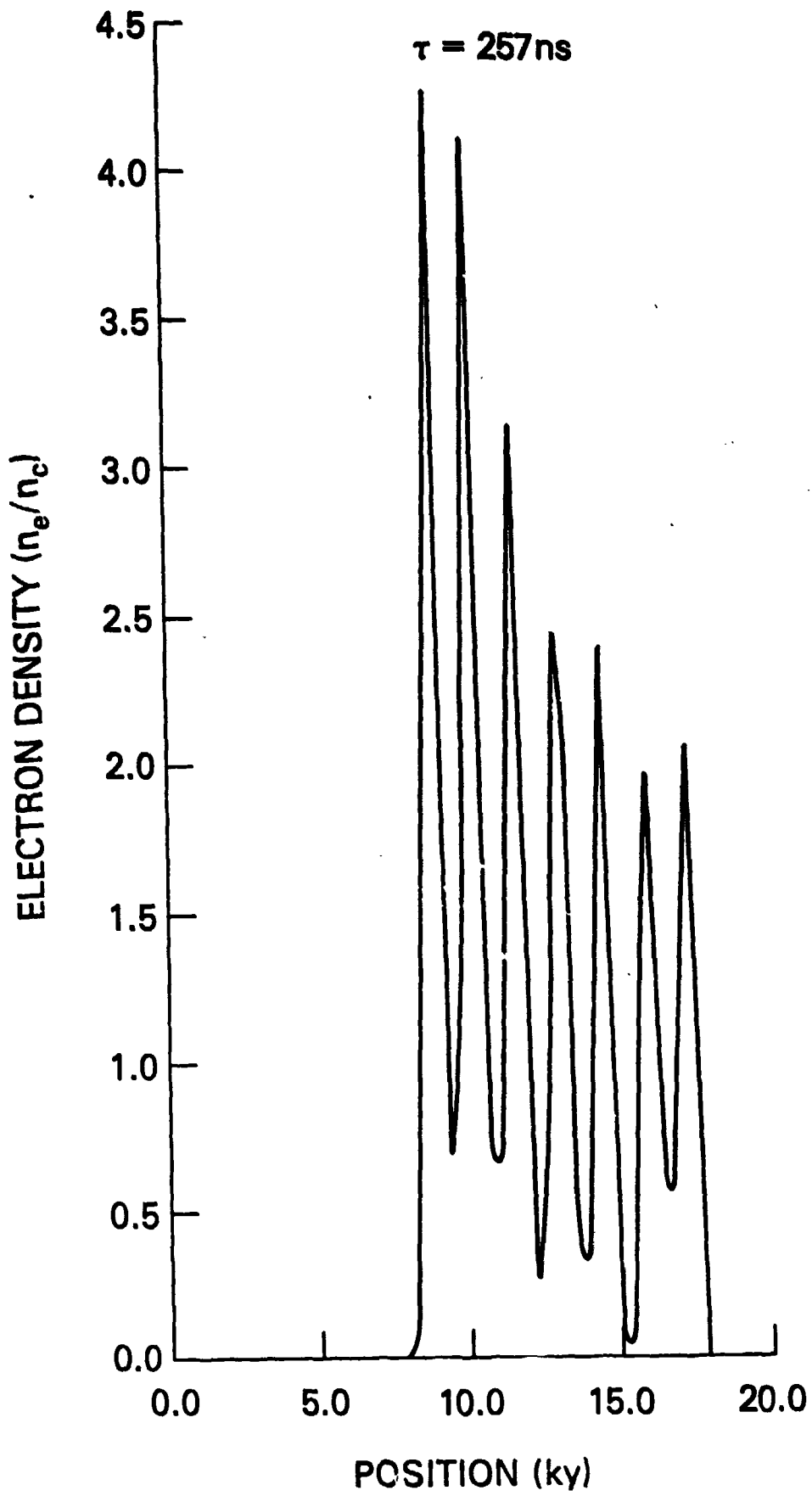


FIGURE 7
C-20

ACKNOWLEDGEMENTS

We would like to acknowledge many useful discussions with Dr. E. A. McLean and Dr. J. R. Greig on optical diagnostics. We also want to acknowledge Dr. T. J. Wieting and J. L. DeRosa for allowing us to use their microwave chamber and for useful technical discussions. The technical assistance of D. Hardesty was greatly appreciated. This work was supported by Naval Sea System Command under a contract to the Naval Research Laboratory.

REFERENCES

1. A. D. MacDonald, Microwave Breakdown in Gases, Wiley, New York, (1966).
2. This technique is also being used to investigate the coupling of energy to surfaces through microwave supported plasmas by T. J. Wieting et al. This work will be discussed in a forth coming publication. T. J. Wieting, J. L. DeRosa, and M. E. Read.
3. C. L. Yee and A. W. Ali, "Microwave Energy Deposition, Breakdown and Heating of Nitrogen and Air," NRL Memo Report 4617, (1981).
4. W. W. Salisbury and W. Flynt, "Microwave Energy Coupling Through Re-entry Plasma," Varo, Inc., RADC-TR-64-575, (December, 1964).
5. W. Beust and W. L. Ford, Microwave J., 4(10), p.91, (1961).
6. Y. P. Raizer, Sov Phy JETP, 34, p.114, (1972).
7. W. E. Scharfman, W. C. Taylor, and T. Morita, IEEE-Trans. Antennas Propag., 12, p.709, (1964).
8. M. E. Read, R. M. Gilgenbach, R. Lucey, K. R. Chu, A. T. Drobot, "Spatial and Temporal Coherence of a 35 GHz Gyromonotron Using the TE_{01} Circular Mode," IEEE Trans. Microwave Theory Tech., 28, p.875, (1980).
9. W. R. Ott, P. Fieffe-Prevost, and W. L. Wiese, Appl. Opt. 12, p.1618, (1973).
10. C. R. Barber, J. Sci. Instrum., 23, p.238, (1946).
11. H. R. Griem, Plasma Spectroscopy, McGraw-Hill, New York, (1964).
12. M. Imami and W. Brost, J. Chem. Phys., 61, p.1115, (1974).
13. R. M. St. John, F. L. Miller, and C. C. Lin, Phys. Rev. A, 134, p.A888, (1964).
14. R. Nicholls, Ann. Geophys., 20, p.144, (1964).
15. W. L. Wiese, M. Smith, and B. M. Glenn, "Atomic Transition Probabilities," Vol. 1, National Bureau of Standards Reference Data Systems NSRDS-NBS-4, (1966).
16. P. Millet, Y. Salamero, H. Brunet, J. Galy and D. Blanc, J. Chem. Phys., 58, p.5839, (1973).
17. C. L. Yee, A. W. Ali, and W. M. Bollen, "Microwave Energy Coupling in a Nitrogen Breakdown Plasma," to be published as an NRL memo.

END